Herbivorous insects independently evolved salivary effectors to regulate plant immunity by destabilizing the malectin-LRR RLP NtRLP4

Xin Wang[1,2], Jia-Bao Lu[1], Yi-Zhe Wang[1], Xu-Hong Zhou[3], Jian-Ping Chen[1,2], Chuan-Xi Zhang[1], Jun-Min Li[1,#], Hai-Jian Huang[1,#]

[1] State Key Laboratory for Quality and Safety of Agro-Products, Key Laboratory of Biotechnology in Plant Protection of MARA, Zhejiang Key Laboratory of Green Plant Protection, Institute of Plant Virology, Ningbo University, Ningbo 315211, China

[2] Institute of Applied Ecology, Fujian Agriculture and Forestry University, Fuzhou 350002, China

[3] Office of Science and Technology, Yunnan University of Chinese Medicine, Kunming 650205, China

Abstract

Plants utilize on receptor-like proteins and receptor-like kinases (RLPs/RLKs) to perceive and respond to a wide variety of invading pathogens and insect herbivores. While the strategies employed by microbial pathogens to suppress plant immunity have been well characterized, it remains unclear how herbivorous insects counteract receptor-mediated defenses. Here, we show that salivary effectors evolve independently in whiteflies and planthoppers to dampen RLP4-mediated plant immunity. RLP4, as a leucine-rich repeat RLP (LRR-RLP), confers plant resistance against herbivorous insects by forming the RLP4/SOBIR1 complexes. In the whitefly *Bemisia tabaci*, BtRDP, the Aleyrodidae-specific salivary sheath protein, interacts with RLP4 from multiple plant species and promotes its ubiquitin-dependent degradation. Overexpression of NtRLP4 in transgenic plants exerts a detrimental effect on *B. tabaci* by exploiting the crosstalk between the salicylic acid (SA) and jasmonic acid (JA) pathways. Conversely, overexpression of BtRDP or silencing of NtRLP4 effectively alleviates such negative effects. In planthopper *Nilaparvata lugens*, the

* Corresponding authors: Jun-Min Li, lijunmin@nbu.edu.cn; Hai-Jian Huang, huanghaijian@nbu.edu.cn

Delphacidae-restricted salivary protein NlSP104 also targets and promotes the degradation of OsRLP4 from rice plants. These findings reveal convergent evolution of salivary proteins in insects, and underscore the complex interactions between plants and herbivorous insects.

Keywords

salivary effector, insect-plant interaction, receptor-like protein, convergent evolution

Introduction

Plants have evolved sophisticated defense systems to withstand continuous threats from microbial pathogens and herbivorous insects. These defenses function at multiple levels, encompassing physical barriers such as the cuticle and cell wall, chemical defenses that include toxic secondary metabolites and anti-nutritive compounds, and indirect defenses involving the emission of herbivore-induced volatiles to attract natural enemies of the herbivores [1, 2]. Beyond these general strategies, plants also rely on the highly specialized molecular immune responses to detect and rapidly respond to invaders. The activation of innate immunity by membrane-localized receptors is a highly conserved mechanism among eukaryotes [3]. In sessile plants, the first line of defense against potential pathogenic microbes or insects relies on cell surface pattern-recognition receptors (PRRs) [4]. The plant genome can encode hundreds of PRRs, including receptor-like kinases (RLKs) and receptor-like proteins (RLPs) [4]. RLKs are consisted of different types of N-terminal ectodomains, a single transmembrane domain, and a cytoplasmic protein kinase domain, while RLPs possess a similar structure but lack the kinase domain [5, 6]. As RLPs lack the intracellular signaling domains, they are anticipated to associate with adaptor kinases to form the bimolecular receptor kinases. For example, suppressor of BAK1-interacting receptor-like kinase 1 (SOBIR1) is reported to act as a common adaptor for most, if not all, of the leucine-rich repeat RLP (LRR-RLP) [6]. Despite the large number of PRRs encoded by plant genomes, only a few of them have been well characterized for their functions in recognizing microbial-associated molecular patterns (MAMPs), damage-associated molecular patterns (DAMPs), and herbivore-associated molecular patterns (HAMPs) [5, 7]. For instance, FLS2 is known to recognize bacterial flagellin [8], EFR can recognize the bacterial elongation factor Tu [9], and EIX2 is responsible for the recognition of the fungal ethylene-inducing xylanase [10].

58 Piercing-sucking insects, such as whiteflies, aphids, and planthoppers, can damage plants by
59 feeding or transmitting viruses. They inject a mixture of saliva into plant tissues, which enhances
60 their feeding efficiency by binding to leaked calcium, degrading extracellular DNA, and regulating
61 plant hormonal signals [11-14]. In response, plants have evolved the ability to detect herbivores by
62 sensing HAMPs present in insect saliva [7, 15]. This triggers pattern-triggered immunity (PTI),
63 including mitogen-activated protein kinase (MAPK) cascades, reactive oxygen species (ROS), and
64 hormone signaling [16-18]. A few salivary proteins have been reported to activate plant PTI, but the
65 specific PRRs that recognize these proteins and trigger plant immunity remain largely unexplored
66 [19-21]. One exception is the inceptin receptor (INR), which is a legume-specific LRR-RLP that
67 can recognize the Vu-In in insect oral secretions [7]. Moreover, plant PRRs have been extensively
68 reported to be targeted by pathogen effectors [22-24]. However, it remains largely unknown how
69 insects cope with plant PRRs.
70 The whitefly *Bemisia tabaci* (Hemiptera: Aleyrodidae) and brown planthopper *Nilaparvata*
71 *lugens* (Hemiptera: Delphacidae) are notorious pests globally. During their feeding process, both
72 insects secrete abundant species-specific salivary proteins into host plants [25, 26]. It is reported
73 that plants initiate defense responses upon the recognition of insect feeding [19, 27]. However, the
74 specific PRRs responsible for this process are still unknown. Both insects can successfully ingest
75 phloem saps with limited plant defenses. At present, it remains unknown how insects attenuate plant
76 defenses. Given that numerous defense mechanisms are conserved across plants [3, 28], it is
77 interesting to investigate whether insect evolves a similar strategy to aid feeding during convergent
78 evolution. In this study, the functions of RLPs in the plant immunity responsive to piercing-sucking
79 insects were investigated, and *B. tabaci* and *N. lugens* were demonstrated to independently evolve
80 salivary proteins to regulate the post-translational modification of RLPs.
81
82 ## Results
83 **BtRDP is most abundantly expressed in salivary glands and secreted into host plants**
84 Based on the transcriptomic analysis, BtRDP (*B. tabaci* RLP-degrading protein; GenBank
85 accession: MN738093) was identified as the most abundantly expressed gene in salivary glands [26].
86 It was a secretory protein featuring an N-terminal signal peptide at the N-terminal, and 6 unique
87 peptides from BtRDP were detected in the *B. tabaci* watery saliva (Fig. S1). As there was no gene

88 homolog identified in the NCBI nr database, BtRDP was subjected to BLAST analysis against the
89 transcriptomic or genomic data of 30 insect species. RDP was distributed in all the analyzed
90 Aleyrodidae species, while no RDP homolog was detected in other species (Table S1). Phylogenetic
91 analysis indicated that RDPs from five *B. tabaci* cryptic species were clustered in the same clad (Fig.
92 S2).

93 A group of *B. tabaci* were allowed to feed on *Nicotiana tabacum* plants for 24 h, and the
94 presence of BtRDP in the infested and non-infested samples were assayed. One band between 26-
95 33 kDa was detected in the *N. tabacum* plants infested by *B. tabaci*, but not in the non-infested
96 plants (Fig. 1a). This band matched the molecular weight of BtRDP identified in the salivary glands,
97 suggesting BtRDP as a salivary protein. According to Western-blotting, qPCR and transcriptomic
98 analysis, BtRDP was nearly exclusively expressed in the salivary glands (Fig. 1b, c; Fig. S3a; Fig.
99 S4). In addition, BtRDP was highly expressed in the adult stages, but lowly expressed in the egg,
100 nymph, and pseudopupa stages (Fig. 1d; Fig. S3b). According to immunohistochemical (IHC)
101 staining, BtRDP was specifically distributed in the principle salivary gland, but not in the accessory
102 salivary gland or other tissues (Fig. 1e). For most piercing-sucking insects, two types of saliva (gel
103 and watery saliva) are secreted into plant tissues . The salivary sheath, formed from gel saliva,
104 serves as an insoluble lining along the stylet path, potentially providing a scaffold for effector
105 delivery [29]. The salivary sheath secreted by *B. tabaci* was also stained with the anti-BtRDP serum.
106 The BtRDP signal was mainly detected in the protuberant structure of sheath (Fig. 1f), suggesting
107 that BtRDP attaches to salivary sheath after secretion.

108

109 **BtRDP is important for *B. tabaci* feeding on tobacco plants**

110 RNA interference was conducted to investigate the role of BtRDP in whitefly feeding.
111 Treatment with ds*BtRDP* efficiently and specifically suppressed the target gene at both the transcript
112 and protein levels (Fig. 2a; Fig. S5). There was no significant difference in the salivary sheath
113 morphology between ds*BtRDP*-treated and ds*GFP*-treated *B. tabaci* (Fig. S6a). However, the
114 salivary sheath length of ds*BtRDP*-treated *B. tabaci* was significantly shorter than that of the
115 ds*GFP*-treated control (Fig. S6b). Furthermore, treatment with ds*BtRDP* did not affect the
116 survivorship of whiteflies (Fig. S6c). A reproduction analysis was conducted, which indicated that
117 the ds*BtRDP*-treated whiteflies oviposited fewer eggs than the control (Fig. 2b). The feeding

behavior of whiteflies was monitored using the electrical penetration graph (EPG) technique, which distinguishes nonpenetration (np), pathway (C), phloem salivation (E1), and phloem ingestion (E2) phases [30] (Fig. S7). Compared to the ds*GFP* control, ds*BtRDP*-treated *B. tabaci* exhibited a significant reduction in phloem ingestion and an extended pathway duration, indicating that BtRDP is necessary for efficient feeding (Fig. 2c).

Salivary proteins are reported to function in intercellular space and/or extracellular space after being secreted into host plants [29, 31]. To investigate the role of BtRDP in different subcellular locations of host plants, we constructed two transgenic *N. tabacum* lines overexpressing BtRDP: one carrying the full-length coding sequence that included the signal peptide (oeBtRDP), which is expected to be secreted into the apoplast (extracellular space), and the other one lacking the signal peptide (oeBtRDP^{-sp}), which is likely to be retained in the cytoplasm. Transgenic plants containing the empty vector (EV), which exerted no significant influence on insect performance compared with the WT (Fig. S8), were used as negative controls. Fecundity and two-choice assays demonstrated that BtRDP, whether localized in the apoplast (oeBtRDP) or cytoplasm (oeBtRDP^{-sp}), enhanced whitefly settling and oviposition relative to the EV controls (Fig. 2d-i; Fig. S9), indicating that BtRDP promotes whitefly feeding behavior irrespective of its subcellular location.

BtRDP interacts with the NtRLP4/NtSORBIR1 complex

To investigate the underlying mechanism of BtRDP in improving whitefly feeding, yeast two-hybrid (Y2H) screening against a *N. benthamiana* cDNA library was conducted using BtRDP^{-sp} as a bait. Totally seven proteins were found to potentially interact with BtRDP^{-sp} (Table S2), including an NbRLP4 (accession Niben261Chr07g1310001.1 in Niben261 genome). NbRLP4 possesses a predicted N-terminal signal peptide, a malectin-like domain, a LRR domain, and a transmembrane domain. NbRLP4 and its closest homology in *N. tabacum* (NtRLP4; GenBank accession: XM_016601109) did not contain the kinase domain (Fig. 3a).

The relative expression of *NtRLP4* in response to *B. tabaci* infestation was investigated. Based on qRT-RCR results, the transcript level of *NtRLP4* was not significantly influenced by *B. tabaci* (Fig. S10). However, a decrease in the protein level of NtRLP4 was detected by Western-blotting assay (Fig. 3b). Pairwise Y2H assays revealed that NtRLP4$_{(23-541)}$ (a truncated version lacking the signal peptide and transmembrane domains) interacted with BtRDP^{-sp} (Fig. 3c). To investigate the

148 specificity of the NtRLP4-BtRDP interaction, another RLP protein NtCf9 with the highest sequence
149 similarity to tomato resistance protein Cf9 (Fig. S11) [32], as well as three randomly selected
150 salivary proteins from *B. tabaci* (BtFTSP, QHB15613; BtSP16.3, MN738005; BtSP37.4,
151 MN738158), were used as controls. As a result, $BtRDP^{-sp}$ did not interact with the truncated NtCf9
152 construct, in which the signal peptide and transmembrane domains were removed (Fig. 3c). Also,
153 $NtRLP4_{(23-541)}$ could not interact with the other three salivary proteins without signal peptides (Fig.
154 S12a, b). These findings raise the question of which domain of NtRLP4 is responsible for binding
155 to BtRDP, as identifying the interacting domain can help to infer where the salivary protein contacts
156 the receptor in plants. We therefore dissected the NtRLP4 domains accordingly. The results showed
157 that it was the LRR domain, rather than the malectin-like domain or the short intercellular region,
158 that was required for the NtRLP4-BtRDP interaction (Fig. 3c). To investigate the shortest LRR
159 sequence responsible for BtRDP interaction, the LRR domain was divided into three segments.
160 However, none of these segments interacted with $BtRDP^{-sp}$ (Fig. S12a). Co-immunoprecipitation
161 (Co-IP) assays further confirmed the specific interaction between BtRDP and NtRLP4 (Fig. 3d). It
162 was the C-terminal myc tag-fused NtRLP4 (NtRLP4-myc), but not the NtCf9 (NtCf9-myc), that
163 could be immunoprecipitated by the C-terminal flag tag fused BtRDP (BtRDP-flag). In the
164 bimolecular fluorescence complementation (BiFC) assay, YFP fluorescence was observed upon co-
165 expression of the N-terminal nYFP tag fused NtRLP4 and N-terminal cYFP tag fused $BtRDP^{-sp}$ (Fig.
166 S12c). Furthermore, in oeBtRDP transgenic plants, endogenous NtRLP4 was specifically
167 immunoprecipitated with BtRDP-flag, which was significantly different from the control (Fig.
168 S12d). These results suggest that BtRDP interacts with NtRLP4.
169 The absence of kinase motifs in the C-terminal region of NtRLP4 suggests that it may function
170 in the cooperation with other proteins to initiate signaling. The receptor-like kinase SOBIR1, which
171 contained a kinase domain (Fig. S13a), has been widely reported to be required for the function of
172 LRR-RLPs in the innate immunity [6]. However, whether SOBIR1 interacted with malectin-LRR
173 RLP remains largely unknown. Through Co-IP assays, our study demonstrated that NtSOBIR1 was
174 capable of interacting with NtRLP4 but not BtRDP (Fig. S13b, c).
175
176 **NtRLP4 and NtSOBIR1 confer resistance to *B. tabaci* infestation**
177 The transgenic *N. tabacum* overexpressing NtRLP4 (oeRLP#1 and oeRLP#2, without any tags)

178 was constructed (Fig. 3e). Compared with the EV control, both oeRLP lines were less attractive to
179 *B. tabaci*, alongside less settling and ovipositing insects (Fig. 3f; Fig. S14a). Also, *B. tabaci* had a
180 significantly decreased fecundity in oeRLP plants (Fig. 3g; Fig. S14b). Similar results were
181 observed after transient overexpression of NtRLP4-GFP in *N. tabacum* (Fig. S14c, d), indicating
182 that NtRLP4 is resistant to *B. tabaci* infestation.

183 Thereafter, the EV and oeRLP#1 plants underwent transcriptomic sequencing (Fig. S15a). A total
184 of 729 differentially expressed genes (DEGs) were identified, comprising 423 up-regulated and 306
185 down-regulated genes (Table S3). Enrichment analysis demonstrated that the majority of up-
186 regulated DEGs were associated with plant-pathogen interaction, environmental adaptation, MAPK
187 signaling pathway, and signal transduction (Fig. S15b). In contrast, the glutathione metabolism,
188 carbohydrate metabolism, and amino acid metabolism pathways were significantly enriched in
189 down-regulated DEGs (Fig. S15c). Noteworthily, numerous DEGs were annotated as RLK/RLP or
190 WRKY transcription factor, with the majority of them being significantly upregulated (Fig. S15d,
191 e). These results suggest an enhanced defense response in oeRLP plants. The crosstalk between
192 salicylic acid (SA) and jasmonic acid (JA) pathways is critical for plant defenses [14]. The increased
193 defense of oeRLP transgenic plants was partially caused by the altered hormonal signaling. The JA-
194 associated gene *FAD7* was significantly induced, while the SA-associated genes *PAL* and *NPR1*
195 were repressed in oeRLP plants (Fig. 3h). Transient overexpression of NtRLP4-GFP in *N. tabacum*
196 plants via *Agrobacterium* infiltration exerted similar effects (Fig. S14e). Furthermore, NtRLP4-GFP
197 significantly enhanced H_2O_2 accumulation (Fig. S14f).

198 The function of NtSOBIR1 was also investigated by transient overexpression and hairpin RNAi
199 (Fig. S16). Overexpression of NtSOBIR1-GFP induced the cell death phenotype five days post agro-
200 injection (Fig. S16). Insects preferred to settle and oviposit on GFP-expressed *N. tabacum* than on
201 NtSOBIR1-GFP-expressed control, even though no obvious death phenotype was observed two
202 days post agro-injection (Fig. S16c, d). For NtSOBIR1 silencing, no cell death phenotype was
203 observed, while the NtSOBIR1-silenced leaves exhibited reduced growth (Fig. S16f). Compared
204 with the EV-silenced control, NtSOBIR1-silenced *N. tabacum* was slightly attractive to *B. tabaci*
205 (Fig. S16g, h). Collectively, these results demonstrate that NtSOBIR1 confers resistance to *B. tabaci*
206 infestation.

207

208 **BtRDP attenuates plant defenses by promoting the degradation of host RLP4**

209 To investigate the interplay between NtRLP4 and BtRDP, transgenic *N. tabacum* silencing
210 NtRLP4 (*RNAi-RLP*#1 and *RNAi-RLP*#2) plants were constructed. Both *RNAi-RLP* lines showed
211 reduced NtRLP4 levels compared with EV plants, with *RNAi-RLP*#2 exhibiting a stronger silencing
212 effect (Fig. S17a). Compared with EV plants, *B. tabaci* showed a tendency to settle on NtRLP4-
213 silenced plants and lay more eggs (Fig. S17b, c). Thereafter, ds*GFP*- and ds*BtRDP*-treated *B. tabaci*
214 were reared on EV, *RNAi-RLP*#1, and *RNAi-RLP*#2, respectively. The ds*BtRDP*-treated *B. tabaci*
215 produced less offspring than the control (decreased by 28.3%; P=0.0007) on EV plants (Fig. 4a),
216 consistent with the results obtained from WT plants (Fig. 2b). On the *RNAi-RLP*#1 plant, the
217 impaired insect reproduction was still observed after ds*BtRDP* treatment, but the extent was slightly
218 reduced (decreased by 23.7%; P=0.002) (Fig. 4a). On the *RNAi-RLP*#2 plant, there was no
219 significant difference between ds*GFP* and ds*BtRDP* treatments (Fig. 4a). The differential rescue
220 effect between the two RNAi lines might result from their different NtRLP4 silencing efficiencies,
221 with the lower NtRLP4 level in *RNAi-RLP*#2 leading to the more complete rescue phenotype (Fig.
222 S17a; Fig. 4a). Collectively, these results suggest that *RNAi-RLP* plants are beneficial for insects
223 and can partially, but not completely, rescue the impaired feeding performance of ds*BtRDP*-treated
224 insects.

225 To investigate the influence of BtRDP on NtRLP4, GFP-tagged NtRLP4 (NtRLP4-GFP) was
226 transiently co-expressed with mCherry-tagged BtRDP (BtRDP-mCherry), red fluorescent protein
227 (RFP)-mCherry, and BtFTSP1-mCherry through agroinfiltration, respectively. All tags were fused
228 with the C-terminal region. As discovered, BtRDP-mCherry did not influence the location patterns
229 of NtRLP4-GFP (Fig. S18). However, a significant reduction in the fluorescent signal of NtRLP4-
230 GFP was detected after co-expression with BtRDP-mCherry, but not with the controls (Fig. S18).
231 Besides, co-expression with BtRDP-mCherry/NtRLP4-GFP significantly reduced H_2O_2
232 accumulation (Fig. 4b), suppressed the expression of JA-associated genes *FAD7* and *PDF.12*, and
233 induced that of the SA-associated genes *PAL* and *NPR1* (Fig. 4c). It was discovered by insect
234 bioassays that, transient overexpression of BtRDP-mCherry rescued the negative effects on whitefly
235 performance caused by NtRLP4-GFP overexpression (Fig. 4d, e). In the host choice experiments,
236 *B. tabaci* displayed a preference for settling on *N. tabacum* leaves co-expressing BtRDP-
237 mCherry/NtRLP4-GFP over those co-expressing RFP-mCherry/NtRLP4-GFP (Fig. 4d). However,

238 almost no preference was observed in *B. tabaci* feeding on *N. tabacum* plants co-expressing BtRDP-
239 mCherry/NtRLP4-GFP and plants expressing GFP alone (Fig. S19).

240 The attenuated NtRLP4-GFP fluorescent signal (Fig. S18), along with the observed decrease
241 in the NtRLP4 protein level during *B. tabaci* infestation (Fig. 3b), led us to speculate on whether
242 BtRDP influenced the accumulation of NtRLP4. To this end, the BtRDP^{-sp}-his and GFP-his proteins
243 were prokaryotically expressed in *Escherichia coli*. Different concentrations of purified BtRDP^{-sp}-
244 his and GFP-his proteins were infiltrated into *N. tabacum* plants overexpressing NtRLP4-myc.
245 Interestingly, the protein level of NtRLP4-myc slightly decreased with the increasing amount of
246 BtRDP^{-sp}-his, while no such effect was observed with GFP-his (Fig. S20). Moreover, the BtRDP^{-sp}-
247 his protein did not have any significant effect on the accumulation of another RLP NtCf9-like (Fig.
248 S20). We further assessed the impact of BtRDP on NtSOBIR1 following NtRLP4 destabilization.
249 As the BtRDP-flag amount increased, NtRLP4-myc accumulation was markedly reduced, while
250 NtSOBIR1-flag levels remained unchanged (Fig. S21).

251 Then, the NtRLP4 levels in oeBtRDP and oeBtRDP^{-sp} plants were detected. Compared with
252 the EV control, a reduced NtRLP4 abundance was observed in both oeBtRDP#1 and oeBtRDP#2
253 transgenic lines, but not in the oeBtRDP^{-sp} plants (Fig. 4f), suggesting the importance of BtRDP
254 secretion in extracellular space. BtRDP attached to salivary sheath localized in plant apoplast (Fig.
255 1f). The presence of signal peptide promoted the secretion of BtRDP into the extracellular space.
256 Therefore, the complete coding region of *BtRDP* was used in subsequent experiments. The NtRLP4-
257 myc and BtRDP-flag were transiently co-expressed in *N. benthamiana* plants through
258 *Agrobacterium* infiltration. As a result, BtRDP-flag significantly decreased the protein level of
259 NtRLP4-myc, but not NtCf9-myc (Fig. 4g). qRT-PCR analyses demonstrated that the transcript
260 level of *NtRLP4* remained unchanged (Fig. S22). These findings indicate that the reduction in the
261 protein level of NtRLP4 is not caused by transcriptional changes but rather by degradation.

262 The ubiquitin system and autophagy are two major pathways regulating protein degradation
263 [33]. At first, MG132, a 26S proteasome inhibitor known to inhibit the degradation of ubiquitin-
264 conjugated proteins, was employed [34]. The results showed that MG132 efficiently prevented the
265 degradation of NtRLP4-myc by BtRDP-flag (Fig. 4h). Then, the autophagy inhibitor 3-
266 Methyladenine (3-MA) and bafilomycin A1 (BAF) that can block autophagy in plants were used
267 [35]. However, the decreased protein level of NtRLP4-myc was still observed in the presence of 3-

268 MA or BAF (Fig. S23). Additionally, NtRLP4-myc and HA-tagged ubiquitin (HA-UBQ) were co-
269 expressed in *N. benthamiana*. Total proteins were extracted from *N. benthamiana* leaves and then
270 subjected to immunoprecipitation with anti-myc beads. The ubiquitin attached to NtRLP4 was
271 determined by immunoblot using the anti-HA antibody. Leaves expressing NtRLP4-myc or UBQ-
272 HA along were used as negative controls. The results showed that a strong UBQ signal was detected
273 in the immunoprecipitated product only when NtRLP4-myc and UBQ-HA were co-expressed (Fig.
274 4i). The molecular weight of UBQ-attached NtRLP4-myc was remarkably larger than that of
275 NtRLP4-myc itself (Fig. 4i). These results suggest that BtRDP promotes NtRLP4 degradation
276 through the ubiquitin system, but not the autophagy pathway.
277
278 **Degrading plant RLP4s by salivary effectors is a common strategy for insects**
279 To investigate the ability of BtRDP to degrade RLPs from other host plants of *B. tabaci*,
280 *Solanum lycopersicum* RLP4 (SlRLP4; GenBank accession: XP_004232910) was selected for
281 further analysis. Sequence analysis revealed a similar gene structure between SlRLP4 and NtRLP4
282 (Fig. S24; Fig. S25a). Moreover, the interaction between BtRDP and SlRLP4 was confirmed
283 through Y2H and Co-IP assays (Fig. S25b, c). Additionally, SlRLP4-myc and SlCf9-like-myc were
284 transiently co-expressed with varying concentrations of BtRDP-flag or GUS-flag, with the myc and
285 flag tags fused with the C-terminus. The results showed that BtRDP-flag exerted no influence on
286 the accumulation of SlCf9-like-myc protein. In contrast, the protein level of SlRLP4-myc was
287 significantly reduced in the presence of BtRDP-flag (Fig. S25d), indicating the conserved function
288 of BtRDP in *B. tabaci* adaptation to different host plants.
289 BtRDP was a gene specific to the Aleyrodidae family, lacking homologues in other species.
290 To explore whether the degradation of RLPs by salivary effectors was a conserved mechanism
291 among different herbivorous insects, a RLP4 homology from *Oryza sativa* (OsRLP4; GenBank
292 accession: XP_015645303; Fig. 5a) and twenty salivary proteins from planthopper species lacking
293 signal peptides were paired to identify the potential interactions using Y2H assays. As a result, only
294 the salivary protein NlSP104^{-sp} (*N. lugens* salivary protein consisting of 104 amino acids, GenBank
295 accession: MF278694) interacted with OsRLP4$_{(29-551)}$ (OsRLP4 lacking signal peptides and
296 transmembrane domains), while the other salivary proteins tested did not show any interaction (Fig.
297 5b, c; Fig. S26). NlSP104 did not exhibit any sequence or structural similarity to BtRDP (Fig. S27).

298 Truncation analysis revealed that NlSP104^{-sp} interacted with both the LRR domain and the malectin-
299 like domain of OsRLP4 (Fig. 5c), which was slightly different from the BtRDP-NtRLP4 interaction
300 (Fig. 3c). Given that both BtRDP and NlSP104 interacted with the LRR domain of RLP4, further
301 investigation focused on the specific region of the LRR domain responsible for NlSP104 binding.
302 The LRR domain of OsRLP4 was divided into three segments, mirroring the division of the LRR
303 domain in NtRLP4 (Fig. S12a). NlSP104^{-sp} interacted with the truncated LRR domain (OsRLP4$_{(480-}$
304 $_{526)}$) (Fig. 5c). In contrast, none of the truncated LRR domain of NtRLP4 interacted with BtRDP^{-sp}
305 (Fig. S12a). Collectively, these findings suggest that the binding sites for salivary proteins to RLP4
306 may differ between *N. lugens* and *B. tabaci*.

307 NlSP104 was a planthopper-specific salivary protein nearly exclusively expressed in salivary
308 glands (Table S1; Fig. 5d; Fig. S28). The function of NlSP104 or its gene homologs in other
309 planthopper species has not been well investigated in previous studies. Silencing NlSP104 did not
310 affect insect survivorship (Fig. 5e). However, significant reductions in honeydew excretion and
311 impaired fecundity were observed in ds*NlSP104*-treated *N. lugens* (Fig. 5f, g), indicating the
312 importance of NlSP104 in insect feeding.

313 Subsequently, OsRLP4-myc was transiently co-expressed with a complete coding region of
314 *NlSP104* (C-terminal flag tagged, NlSP104-flag). Another salivary protein NlSP7-flag and NtCf9-
315 myc were used as negative controls. It was found that NlSP104-flag specifically and significantly
316 decreased the protein level of OsRLP4-myc, which differed significantly from that of the NlSP7-
317 flag (Fig. 5h). Additionally, NlSP104-flag failed to decrease the protein level of NtCf9-myc (Fig.
318 5h). These findings suggest that *N. lugens* potentially evolves salivary effectors to target rice RLPs.
319

320 **Discussion**

321 Plants have evolved a complex innate immune system to protect themselves against
322 pathogen/insect invasion, and the cell surface-localized PRRs function on the frontline [4]. To
323 counteract this response, the pathogens have developed various strategies to avoid plant PRR-
324 mediated PTI for their own advantage [36]. However, it remains unknown whether insects take the
325 similar strategy to sabotage plant immunity. In this study, we demonstrate that the RLP4 confer plant
326 resistance against herbivorous insects. In response, both planthoppers and whiteflies secrete salivary
327 effectors to facilitate the degradation of defensive RLP4, leading to the attenuated plant immunity.

328 Our results suggest that manipulation of PRRs may be a conserved strategy for herbivorous insects.

329 PRRs detect modified-self or non-self patterns and initiate a cascade of immune signaling
330 events, which subsequently regulate downstream defense responses, conferring plant resistance
331 against invaders [4, 5]. Although various insect salivary components have been identified as triggers
332 for plant immune responses, the specific PRRs involved in this process remain unclear. Our study
333 indicates that RLP4 significantly influences insect performance by modulating plant hormones and
334 ROS (Fig. 3f-h; Fig. S14), highlighting the critical role of RLP4 in plant immunity. However, the
335 precise ligand for RLP4 has yet to be identified. The malectin-LRR receptor RLP4 may respond to
336 the DAMPs or HAMPs released during insect feeding [37], a hypothesis that warrants further
337 investigation. RLP4 lacks an intracellular kinase domain, and instead forms bimolecular receptor
338 kinases by interacting with SOBIR1 (Fig. S13). Silencing of NtRLP4 or NtSOBIR1 in *N. tabacum*
339 attracts *B. tabaci* and promotes insect reproduction, whereas overexpression of either gene exerts
340 the opposite effect (Fig. S14-S17). The association between RLPs and SOBIR1 protein kinases is
341 structurally and functionally analogous to that of genuine receptor kinases [6]. Therefore,
342 destabilizing the RLP4/SOBIR1 complex can potentially disrupt the immune recognition processes.
343 Noteworthily, although NtRLP4 interacts with SOBIR1, this alone does not confirm that it operates
344 strictly through this canonical module. Evidence from other RLPs shows that co-receptor usage can
345 be flexible, and some RLPs function partly or conditionally independent of SOBIR1 [38]. Therefore,
346 a more definitive assessment of NtRLP4 signaling will therefore require genetic dissection of its co-
347 receptor dependencies, including but not limited to SOBIR1.

348 As pivotal regulators in immune signaling, PRRs are frequently targeted by multiple pathogens
349 through diverse mechanisms. For example, *Pseudomonas syringae* hampers the functionality of
350 receptor complexes by disrupting the ligand-dependent association between receptor-like kinase
351 BAK1 and the flagellin receptor FLS2 [24], while *Phytophthora infestans* promotes alternative
352 splicing of the host RLPKs to enhance infection [23]. PRRs are usually subjected to degradation via
353 post-translational modifications [39]. In plants, the activity and stability of PRRs are under stringent
354 regulation since excessive activation of PRRs could be detrimental [22, 40]. One prevalent
355 regulatory mechanism involves ubiquitination followed by subsequent degradation mediated by the
356 26S proteasome [39]. Mounting evidence has demonstrated that bacteria, fungi, viruses, and
357 oomycetes exploit such mechanisms to facilitate PRR degradation [41-44]. Nevertheless, the

358 occurrence of effector-mediated PRR degradation in insects is unreported. Our study reveals that
359 the salivary effectors BtRDP from *B. tabaci* and NlSP104 from *N. lugens* interacts with plant RLP4s,
360 resulting in their degradation in a ubiquitin-dependent manner (Fig. 4f-i).

361 Notably, BtRDP and NlSP104 exhibit neither sequence nor structural similarity and do not
362 resemble the known eukaryotic ubiquitin-ligase domains. Their interaction with RLP4s occurs in
363 the extracellular space (Fig. 3d; Fig. 5c), whereas the ubiquitin-proteasome system primarily
364 functions within the cytosol and nucleus [45]. Furthermore, NtRLP4 reduction is observed only in
365 oeBtRDP transgenic plants, not in oeBtRDP^{-sp} plants (Fig. 4f), indicating that BtRDP exerts its
366 influence on NtRLP4 in the extracellular space. These observations collectively refute the
367 possibility that BtRDP or NlSP104 possesses the intrinsic E3 ligase activity capable of directly
368 ubiquitinating RLP4s within plant cells. Importantly, the reduced NtRLP4 levels may not stem from
369 a direct physical interaction between BtRDP and NtRLP4. Instead, BtRDP may indirectly affect
370 RLP4 post-translational modification, thereby accelerating its degradation, which warrants further
371 investigation. Additionally, the independent evolution of RLP4-targeting effectors in various insect
372 lineages may expedite plant-insect co-evolution. Plants with robust RLP4-mediated defenses can
373 select for herbivores carrying effective effectors, driving an evolutionary "arms race". Conversely,
374 insects targeting similar host proteins may exert parallel selective pressures on unrelated plant
375 species, potentially shaping defense diversification across plant communities. Understanding these
376 dynamics provides insight into how molecular interactions scale up to influence herbivore
377 adaptation, host range, and the ecological outcomes of plant-insect interactions.

378 Herbivorous insects employ a mix of salivary components to ensure successful feeding [29].
379 Previous research has indicated that *B. tabaci* suppresses plant defenses by utilizing SA-JA crosstalk,
380 with the salivary protein Bt56 playing a crucial role in this process [14]. Bt56 activates the SA-
381 signaling pathway by directly interacting with a KNOTTED 1-like homeobox transcription factor
382 [14]. This study investigates the effects of another salivary effector, BtRDP, on plant hormones, and
383 finds that it elicits similar effects to Bt56, albeit primarily impacting the signal recognition process
384 (Fig. 3h; Fig. S14e). This leads us to speculate that different salivary effectors from the same insect
385 species may simultaneously target the same signaling pathway to ensure effective immune
386 suppression. Our analysis reveals that BtRDP interacts with other host genes apart from NtRLP4
387 (Table S2), and silencing NtRLP4 cannot completely rescue the impaired feeding performance of

388 ds*BtRDP*-treated insects (Fig. 4a). Salivary proteins exert a crucial effect on mediating the
389 interactions between herbivores and plants. The dynamic interplay between plants and insects may
390 be highly complex, one salivary protein can target multiple plant pathways, and one plant pathway
391 is influenced by multiple salivary proteins.

392 Together, this study reveals that suppressing PRR-mediated plant immunity may be a
393 conserved strategy employed by herbivorous insects for successful feeding. We demonstrate that
394 whiteflies and planthoppers have independently evolved salivary effectors that facilitate the
395 ubiquitin-dependent degradation of defensive RLP4 in host plants, thereby dampen RLP4-mediated
396 plant immunity (Fig. 6). Nevertheless, the precise mechanism by which RLP4 contributes to plant
397 defense warrants further consideration. While it may function as a canonical PRR that perceives
398 insect-derived molecular patterns, several lines of evidence point to an alternative interpretation.
399 Structurally, RLP4 differs from classical LRR-RLP: it contains a malectin-like domain and a
400 relatively small LRR domain, contrasting with typical LRR-RLPs that often possess large LRRs
401 dedicated to ligand binding. Functionally, NtRLP4 overexpression lines exhibit significantly altered
402 transcriptional profiles and dysregulated SA/JA pathways even in the absence of insect infestation,
403 a phenotype inconsistent with canonical PRRs, which typically remain quiescent until ligand
404 perception. These findings point to an alternative explanation: rather than functioning as a classical
405 PRR that recognizes insect-derived molecules, RLP4 may act as a regulatory component within
406 plant immune signaling networks. Elucidating the precise mechanism of RLP4 in conferring plant
407 defense against herbivorous insects will therefore be an important focus of future research.

408

409 ## Material and methods

410 **Insects and plants**

411 A colony of *B. tabaci* (cryptic species MED) was originally collected from a soybean field in
412 Suzhou, Anhui Province, China. The insects were subsequently maintained on *N. tabacum* cv. K326
413 plants under controlled laboratory conditions (25 ± 1 °C, 50–70% relative humidity, 16:8 h
414 light:dark photoperiod). For experimental use, *N. benthamiana* and *N. tabacum* plants were grown
415 in a climate-controlled growth chamber (23 ± 1 °C, 16:8 h light: dark cycle).

416

417 **Phylogenetic analysis of RDP**

418 To identify potential RDP homologs across insect species, we performed a BLASTp search using
419 the BtRDP protein sequence as a query against the predicted proteomes of 30 insect species. Hits
420 were filtered using an E-value cutoff of 10^{-5}. The retrieved RDP homologs were aligned using
421 MAFFT (v7.310) with default parameters [46]. To improve alignment quality, we removed
422 ambiguously aligned regions using Gblocks with default settings. The optimal amino acid
423 substitution model (JTT+G) was determined using ModelTest-NG (v0.1.6). Phylogenetic
424 relationships were inferred using maximum likelihood analysis in RAxML (v0.9.0) with 1000
425 bootstrap replicates to assess branch support [47]. The final tree was visualized and annotated using
426 iTOL (https://itol.embl.de/).
427
428 **Preparation of anti-BtRDP and anti-NtRLP4 serum**
429 The coding sequence of BtRDP (excluding the signal peptide) was PCR-amplified and cloned
430 into the pET-28a vector (Novagen) to generate a C-terminal 6×His-tagged fusion protein. The
431 recombinant plasmid was transformed into *Escherichia coli* Transetta (DE3) competent cells
432 (TransGen Biotech, Beijing, China). Protein expression was induced with 0.5 mM isopropyl-β-D-
433 thiogalactoside (IPTG) at 28°C for 8 h. Bacterial cells were harvested by centrifugation and lysed
434 via ultrasonication for 30 min. The recombinant $BtRDP^{-sp}$-His protein was purified under native
435 conditions using Ni-NTA agarose (Qiagen, Hilden, Germany) according to the manufacturer's
436 protocol.
437 Purified $BtRDP^{-sp}$-His protein was used to immunize rabbits (Hua'an Biotechnology,
438 Hangzhou, China) for custom polyclonal antibody production. The anti-NtRLP4 serum, prepared
439 by immunizing rabbits with peptide GQNSDRPISTKNST, was produced via the custom service of
440 Genscript Biotechnology Company (Nanjing, China). The anti-BtRDP serum was subsequently
441 conjugated to Alexa Fluor™ 488 NHS Ester (#A20000, Thermo Fisher Scientific) following
442 standard labeling protocols.
443 The specificity of anti-BtRDP serum was tested by comparing ds*GFP*- and ds*BtRDP*-treated
444 *Bemisia tabaci*. The results showed that ds*BtRDP* significantly reduced the target gene. Similarly,
445 the specificity of anti-NtRLP4 serum was tested by comparing RNAi-EV and RNAi-NtRLP4 plants,
446 which showed a reduced NtRLP4 expression in *RNAi-NtRLP4* plants.
447

448 **Immunohistochemistry (IHC) staining**

449 Dissected *B. tabaci* heads with attached salivary glands and Parafilm-embedded salivary
450 sheaths were fixed in 4% paraformaldehyde (#E672002, Sango Biotechnology, Shanghai) for 30
451 min. Salivary sheaths adherent to Parafilm were similarly excised and fixed under identical
452 conditions. After fixation, samples were washed three times with PBST (PBS containing 0.1%
453 Tween-20) and blocked with 10% FBS for 2 h at room temperature. The tissues were then incubated
454 overnight at 4°C with Alexa Fluor 488-conjugated anti-BtRDP serum (1:200 dilution), followed by
455 co-staining with phalloidin-rhodamine (1:500, Thermo Fisher Scientific) for 30 min and 4',6-
456 diamidino-2-phenylindole (DAPI) solution (#ab104139, Abcam, Cambridge, USA) for nuclear
457 visualization. Fluorescent images were acquired using a Leica SP8 confocal microscope (Leica
458 Microsystems) to examine BtRDP localization patterns

459

460 **Protein extraction and Western-blotting assays**

461 To identify secreted salivary proteins in *N. tabacum* plants, approximately 200 *B. tabaci* adults
462 were confined in a 3-cm diameter feeding cage and allowed to feed on host plants for 24 h. After
463 feeding, the eggs deposited on the infested tobacco leaves were removed. The leaves showing no
464 visible insect contamination were immediately frozen in liquid nitrogen and ground to a fine powder.
465 The powdered tissue was then homogenized in RIPA Lysis Buffer (#89900, Thermo Fisher
466 Scientific) for protein extraction. To examine the effects of insect feeding on NtRLP expression,
467 groups of approximately 200 *B. tabaci* were allowed to feed on 4-5 true-leaf stage tobacco plants
468 for 12, 24, or 48 h, with uninfested plants serving as controls. For silencing/overexpression
469 efficiency tests, leaf samples were collected at 48 h post-*Agrobacterium* infiltration, along with
470 transgenic tobacco plants at the 4-5 true-leaf stage. For insect tissue analysis, various *B. tabaci*
471 organs were carefully dissected in 1×PBS buffer, including carcasses (20), fat bodies (20), guts (40),
472 salivary glands (60), and ovaries (10), with sample sizes indicated in parentheses. All dissected
473 tissues were transferred to lysis buffer for protein extraction. Total protein concentrations in both
474 insect and plant homogenates were quantified using a BCA Protein Assay Kit (#CW0014S,
475 CwBiotech, Taizhou, China). Equal protein amounts were separated by SDS-PAGE and electro-
476 transferred to PVDF membranes.

477 Membranes were probed with the following primary antibodies: anti-FLAG (1:10,000, #MA1-

478 91878, Thermo Fisher Scientific), anti-MYC (1:10,000, #MA1-21316, Thermo Fisher Scientific),
479 anti-GFP (1:10,000, #MA5-15256, Thermo Fisher Scientific), anti-NtRLP4 (1:5,000, GenScript
480 Biotechnology, Nanjing, China), and anti-BtRDP serum (1:5,000, Huaan Biotechnology, Hangzhou,
481 China). Following primary antibody incubation, membranes were treated with HRP-conjugated
482 secondary antibodies: goat anti-mouse IgG (1:10,000, #31430, Thermo Fisher Scientific) or goat
483 anti-rabbit IgG (1:10,000, #31460, Thermo Fisher Scientific). Protein bands were visualized using
484 an AI 680 image analyzer (Amersham Pharmacia Biotech, Buckinghamshire, UK), with Ponceau S
485 staining used to verify equal protein loading.
486
487 **Quantitative real-time PCR (qRT-PCR) analysis**
488 To prepare tissue-specific samples from *B. tabaci*, adult females were dissected to isolate
489 carcasses (10), fat bodies (10), guts (20), salivary glands (40), and ovaries (10). Additionally,
490 different developmental stages, including eggs (50), nymphs (20), pupae (20), and adult males (20)
491 and females (20), were collected for analysis. The number of insects in each sample is indicated in
492 parentheses. To extract RNA from *N. tabacum* plants, the samples were grinded using liquid
493 nitrogen after collection. Total RNA was extracted using the TRIzol Total RNA Isolation Kit (#9109,
494 Takara, Dalian, China) following the manufacturer's instructions. RNA purity and concentration
495 were assessed using a NanoDrop spectrophotometer (Thermo Fisher Scientific). First-strand cDNA
496 was synthesized from equal amounts of RNA (1 μg) using the HiScript II Q RT SuperMix (#R212-
497 01, Vazyme, Nanjing, China). Gene expression analysis was performed using a Roche LightCycler®
498 480 system (Roche Diagnostics, Mannheim, Germany) with SYBR Green Supermix (#11202ES08,
499 Yeasen, Shanghai, China). The thermal cycling protocol consisted of initial denaturation at 95°C for
500 5 min, and amplification for 40 cycles of 95°C for 10 s and 60°C for 30 s. Primers were designed
501 with Primer Premier v6.0 (Table S4). *B. tabaci Tubulin* and *N. tabacum Tubulin* served as internal
502 controls for normalization. Relative gene expression was calculated using the $2^{-\Delta\Delta Ct}$ method [48].
503 Three to six independent biological replicates, each repeated twice, were performed.
504
505 **RNA interference**
506 The target gene DNA sequences were amplified using primers listed in Table S4 and
507 subsequently cloned into the pClone007 Vector (#TSV-007, Tsingke Biotechnology, Beijing, China).

508 For dsRNA production, PCR-generated DNA templates containing T7 promoter sequences were
509 transcribed *in vitro* using the T7 High Yield RNA Transcription Kit (#TR101-01, Vazyme Biotech,
510 Nanjing, China). The RNAi experiments were performed according to established methods [49].
511 Briefly, newly emerged adult whiteflies were anesthetized with carbon dioxide for 5-10 seconds.
512 Approximately 50 nL of dsRNA solution (2 μg/μL) was microinjected into the mesothorax of each
513 insect using a FemtoJet microinjection system (Eppendorf, Hamburg, Germany). Following
514 injection, the whiteflies were maintained on healthy *N. tabacum* leaves under standard rearing
515 conditions. Only actively moving insects were selected for subsequent analyses. Gene silencing
516 efficiency was evaluated on day 4 post-injection using both qRT-PCR and Western-blotting
517 approaches.
518
519 **Generation of transgenic plants**
520 We generated two transgenic *N. tabacum* lines expressing different BtRDP variants: one
521 containing the full coding sequence (oeBtRDP) and another lacking the signal peptide (oeBtRDP^{-}
522 ^{sp}), which may affect protein secretion. The target sequences, along with the full-length NtRLP4
523 coding sequence and an NtRLP4 hairpin RNAi construct, were each cloned into the pBWA(V)HS
524 vector. The oeBtRDP and oeBtRDP^{-sp} were fused with C-terminal flag tags, while no tag was fused
525 to oeNtRLP4. All constructs were transformed into *A. tumefaciens* strain GV3101 and used to
526 generate transgenic tobacco plants (K326 background) through *Agrobacterium*-mediated
527 transformation performed by Wuhan Boyuan Biological Company. Transgenic lines were verified
528 by qRT-PCR and western blotting, with empty vector-transformed plants serving as controls, and
529 two independent lines for each construct were selected for further experiments.
530
531 **Target gene silencing in plants**
532 The hairpin RNAi construct targeting *NtSOBIR1* was generated by cloning the specific
533 fragment into the pBWA(V)HS plasmid using BsaI and Eco31I restriction enzymes. The
534 recombinant vector was then transformed into *A. tumefaciens* strain GV3101 and subsequently
535 infiltrated into *N. tabacum* leaves using the agroinfiltration method. Following a 48-h incubation
536 period under standard growth conditions, silencing efficiency was quantitatively evaluated by qRT-
537 PCR analysis.

538

539 **Transcriptomic sequencing**

540 To investigate the transcriptional effects of NtRLP4, BtRDP, and BtRDP^{-sp} in *N. tabacum*, leaf
541 samples from EV, oeRLP4#1, oeBtRDP#1, and oeBtRDP^{-sp}#1 transgenic plants were homogenized
542 in TRIzol Reagent (#10296018, Invitrogen, Carlsbad, CA, USA) for total RNA extraction following
543 the manufacturer's protocol. Afterwards, total RNA was extracted according to the instructions of
544 the manufacturer, and the RNA samples were sent to Novogene Institute (Novogene, Beijing, China)
545 for transcriptomic sequencing. Briefly, poly(A)+ RNA was isolated from 20 μg pooled total RNA
546 using oligo(dT) magnetic beads, followed by fragmentation in divalent cation buffer at 94°C for 5
547 min. First-strand cDNA synthesis was performed using N6 random primers, with subsequent
548 second-strand synthesis to generate double-stranded cDNA. After end-repair and Illumina adapter
549 ligation, the products were PCR-amplified (15 cycles) and purified using a QIAquick PCR
550 Purification Kit (#28104, Qiagen, Hilden, Germany). The resulting cDNA libraries were quantified
551 and quality-checked before paired-end sequencing on an Illumina NovaSeq 6000 platform. All raw
552 sequencing data were deposited in the National Genomics Data Center under accession number
553 PRJCA025907.

554

555 **Analysis of transcriptomic data**

556 The raw sequencing reads were quality-filtered using Illumina's internal software, and the
557 resulting clean reads from each cDNA library were aligned to the *N. tabacum* reference genome in
558 Sol Genomics Network
559 (https://solgenomics.net/ftp/genomes/Nicotiana_tabacum/edwards_et_al_2017/) using HISAT
560 v2.1.0 [50]. Low-quality alignments were removed using SAMtools (v1.7) with default parameters
561 [51]. Transcript abundance was quantified as Transcripts Per Million (TPM) using Cufflinks (v2.2.1)
562 [52]. Differential expression analysis was performed with DESeq2 (v2.2.1) [53], identifying
563 significantly DEGs using thresholds of |log2(fold change)| > 1 and adjusted p-value < 0.05. PCA of
564 transcriptome profiles was conducted using a custom R script plotPCA (github.com/franco-
565 ye/TestRepository/blob/main/PCA_by_deseq2.R). For functional annotation, KEGG pathway
566 enrichment analysis was performed in TBtools (v2.083) using a one-sided hypergeometric test:

567 $P = 1 - \sum_{i=0}^{m-1} \left(\frac{\binom{M}{i}\binom{N-M}{n-i}}{\binom{N}{n}} \right)$, [54]. In this software, enriched *P*-values were calculated according to
568 one-sided hypergeometric test: with *N* representing the number of gene with KEGG annotation, *n*
569 standing for the number of DEGs in *N*, *M* indicating the number of genes in each KEGG term, and
570 *m* suggesting the number of DEGs in each KEGG term.
571
572 **Insect bioassays**
573 To survivorship analysis, newly emerged *B. tabaci* adults were microinjected with dsRNA and
574 placed on *N. tabacum* leaves. After 24 h, any dead individuals (potentially due to injection injury)
575 were removed. For each treatment, 20-30 surviving adults were transferred to leaf cages, and
576 mortality was recorded daily for 10 days. Three independent biological replications were performed.
577 For fecundity analysis, dsRNA-treated virgin females were paired with untreated males in
578 leaf cages. Five such pairs were maintained per cage (n=10-12 cages per treatment). Egg deposition
579 was quantified daily for 3 consecutive days under controlled conditions. Each male-female pair was
580 considered an experimental replicate.
581 For host preference test, detached *N. tabacum* leaves with moist cotton-wrapped petioles were
582 arranged in a 50-cm diameter choice arena with a central release chamber. Forty adult whiteflies
583 were released per chamber, and settling preference was recorded at 3, 6, 12, 24, 36, and 48 h post-
584 release. The experiment included 10-12 replicates per treatment, with leaf positions randomized
585 between replicates to eliminate positional bias.
586
587 **EPG recording and analysis**
588 Feeding behavior of *B. tabaci* was monitored using a GiGA-8d EPG amplifier (Wageningen
589 Agricultural University; 10 TΩ input resistance, <1 pA input bias current) with 50× gain and ±5 V
590 output range. Prior to recording, dsRNA-treated whiteflies were starved for 12 h on moist filter
591 paper, briefly anesthetized with CO_2 (10 s), and connected to the amplifier via a gold wire electrode
592 (20 μm diameter × 5 cm length) attached to the pronotum using conductive silver glue. Plant
593 electrodes consisted of copper wires (2 mm diameter × 10 cm length) inserted into the soil of potted
594 *N. tabacum*. Recordings were conducted for 8 h in a Faraday cage (120×75×67 cm; Dianjiang,
595 Shanghai), with only insects surviving the full duration retained for analysis.

596 Recorded waveforms were processed using PROBE 3.4 software (Wageningen Agricultural
597 University) and categorized into four distinct feeding phases: nonpenetration (np), pathway duration
598 (C), phloem salivation (E1), and phloem ingestion (E2) as defined in a previous study [30]. Each
599 treatment included ⩾10 biological replicates, with ds*GFP*-injected and untreated whiteflies
600 serving as controls.
601
602 ***Agrobacterium*-mediated plant transformation in *N. tabacum* and *N. benthamiana***
603 The recombinant expression vectors were introduced into *A. tumefaciens* strain GV3101 via
604 heat shock transformation. Transformed cells were selected on LB agar plates supplemented with
605 50 μg/mL kanamycin and 10 μg/mL rifampicin, followed by incubation at 28°C for 60 h. Positive
606 colonies were inoculated into liquid LB medium with the same antibiotics and grown to log phase.
607 Bacterial cells were then pelleted by centrifugation at 2,400 *g* for 2 min and resuspended in induction
608 buffer (10 mM $MgCl_2$, 10 mM MES [pH 5.6], 200 μM acetosyringone) adjusted to specific OD_{600}
609 values depending on the experiment.
610 For standard experiments, bacterial suspensions were normalized to OD_{600} = 1.0, while
611 degradation assays used three concentrations (OD_{600} = 0.05, 0.3, and 1.0). Equal volumes of selected
612 bacterial suspensions were mixed and infiltrated into leaves of 4–5-week-old *N. tabacum* and *N.*
613 *benthamiana* plants using a needleless syringe. Infiltrated plants were maintained under controlled
614 conditions for subsequent analysis.
615
616 **Diaminobenzidine (DAB) staining**
617 To detect H_2O_2 accumulation in *N. tabacum* leaves, leaf samples were immersed in 1 mg/mL
618 3,3'-diaminobenzidine tetrahydrochloride (DAB-HCl, #D8001, Sigma-Aldrich, St. Louis, MO,
619 USA) solution (pH 3.8) for 6 hours at room temperature, allowing H_2O_2-dependent brown
620 polymerization to occur. Following incubation, the DAB solution was replaced with 100% ethanol
621 for chlorophyll removal, and samples were decolorized overnight at 65°C. The destained leaves
622 were then photographed under standardized conditions using a Canon EOS 80D digital camera
623 (Canon Inc., Tokyo, Japan).
624
625 **Interaction assays between two proteins**

626 In the Y2H screening assay, the coding sequence of BtRDP^{-sp} was cloned into the pGBKT7
627 bait vector (Clontech, USA), while a *N. benthamiana* cDNA library was constructed in the pGADT7
628 prey vector (Biogene Biotech, Shanghai, China). These recombinant vectors were co-transformed
629 into yeast strain Y2HGold and plated on QDO medium (SD/-Ade/-His/-Leu/-Trp, #630428, Takara)
630 for 3 days at 30°C. Positive colonies were cultured in QDO liquid medium, and plasmids were
631 extracted using a yeast DNA kit (#DP112-02, TIANGEN, Beijing, China) before transformation
632 into E. coli DH5α (#TSC-C14, Tsingke) for sequencing (YouKang Biotech, China) to identify
633 interacting partners.

634 In the pairwise Y2H verification assay, BtRDP^{-sp} and NlSP104^{-sp}, and mutant variants of
635 NtRLP4/SlRLP4/OsRLP4 were cloned into either pGBKT7 or pGADT7 vectors using primers from
636 Table S4. Given that Y2H is generally difficult to identify membrane receptors, the truncated
637 versions of NtRLP4/SlRLP4/OsRLP4 lacking the signal peptide and transmembrane domains were
638 used. Yeast co-transformants were first selected on DDO medium (SD/-Leu/-Trp) (#630417, Takara)
639 for 3 days at 30°C, then spotted onto QDO medium to confirm interactions through growth after
640 another 3 days of incubation.

641 In the Co-IP assays, Full-length sequences of *BtRDP*, *NlSP104*, *NtSOBIR1*, *NtRLP4*, *SlRLP4*,
642 and *OsRLP4* were cloned into lic-myc or lic-flag vectors for C-terminal tagging, with BtFTSP-flag
643 serving as a negative control. Five-week-old *N. benthamiana* leaves were agroinfiltrated with these
644 constructs or collected from oeBtRDP transgenic plants. Total proteins were extracted from 1 g
645 frozen tissue in IP lysis buffer (#87788, Thermo Scientific) with protease inhibitors (#56079200,
646 Roche, Switzerland), followed by centrifugation at 1,000 × *g* for 20 min. Cleared lysates were
647 incubated with anti-flag beads (#L00432-1, GenScript, Nanjing, China) for 4 h at 4°C, washed with
648 PBS, and eluted in 2× SDS-PAGE buffer (500 mM Tris-HCl, pH=6.8, 50% glycerin, 10% SDS, 1%
649 bromophenol blue, and 2% β-mercaptoethanol) for Western-blotting assay.

650 In the BiFC assay, BtRDP^{-sp}, BtFTSP^{-sp}, NtRLP4, and NtCf9-like were cloned into the pCV-
651 cYFP or pCV-nYFP vectors, respectively. After transforming *A. tumefaciens* GV3101, pairwise
652 combinations were co-infiltrated into *N. benthamiana* leaves. Following 36-48 h incubation in a
653 growth chamber, reconstituted YFP fluorescence was visualized using a Leica SP8 confocal
654 microscope with standard filter sets for YFP detection.

655

656 **RLP degradation by salivary effectors among different herbivorous insects**

657 To examine salivary protein effects on RLPs, we co-infiltrated *A. tumefaciens* GV3101 strains
658 carrying various constructs into *N. benthamiana* leaves. The recombinant vectors expressed C-
659 terminally tagged proteins: BtRDP-flag, NlSP104-flag, GUS-flag, NlSP7-flag, and myc-tagged
660 RLPs (NtRLP4, SlRLP4, OsRLP4, SlCf9, NtCf9). Bacterial suspensions were mixed at
661 predetermined OD_{600} ratios before infiltration, with leaf samples collected 48 hours post-infiltration
662 for subsequent analysis.

663 For confocal microscopy studies, *N. benthamiana* leaves were co-infiltrated with *A.*
664 *tumefaciens carrying*: (1) NtRLP4-GFP plus BtRDP-mCherry, (2) NtRLP4-GFP plus RFP-mCherry,
665 or (3) NtRLP4-GFP plus BtFTSP-mCherry. The samples were imaged by confocal microscopy at
666 48 h post injection. The same parameters were used in photographing.

667 This study also conducted a treatment on *N. benthamiana* plants that were overexpressing
668 NtRLP4-myc using purified proteins. Briefly, the $BtRDP^{-sp}$ and GFP coding sequences were cloned
669 into pET-28a for 6×His-tagged expression in *E. coli* Transetta (TransGen Biotech). Protein
670 expression was induced with 0.5 mM IPTG at 25°C for 8 h, followed by purification using Ni-NTA
671 agarose and buffer exchange into PBS using a 3-kDa molecular-weight cutoff Amicon Ultra-4
672 Centrifugal Filter Device (Millipore, MA, USA). Different concentrations of purified proteins were
673 infiltrated into leaves of *N. benthamiana* plants stably expressing NtRLP4-myc, with samples
674 collected 24 h post-treatment.

675 To investigate degradation pathways, we infiltrated *N. benthamiana* leaves with: 50 μM
676 MG132 (#M7449, Sigma-Aldrich, Steinheim, Germany), 5 μM 3-MA (#M9281, Sigma-Aldrich,),
677 or 10 nM BAF (#BML-CM110-0100, Enzo Life Sciences, Farmingdale, USA) at 24 h post-
678 agroinfiltration. The samples were incubated for additional24 h. Protein levels were detected using
679 Western-blotting assay.

680

681 ***In planta* ubiquitination assay**

682 Ubiquitination detection in *N. benthamiana* was performed according to the methods
683 previously reported [55]. The recombinant vector for transient expression of the HA-fused ubiquitin
684 protein was kindly provided by Dr. Chao Zheng (Ningbo University). Myc-tagged proteins were co-
685 expressed with HA-UBQ by agroinfiltration, and 50 μM MG132 was injected into the *N.*

686 *benthamiana* leaves one day post *A. tumefaciens* infiltration. Immunoprecipitation was performed
687 using anti-myc beads (ytma-20, ChromoTek , Planegg-Martinsried, Germany). Ubiquitination
688 signals were detected by immunoblot with anti-HA antibody (HT301, TransGen Biotech, Beijing,
689 China).
690
691 **Scanning electron microscopy (SEM)**
692 *B. tabaci* adults were allowed to feed on artificial diet solutions for 24 h. Parafilm sections
693 containing salivary sheaths were carefully excised and rinsed with 1× PBS (pH 7.4) to remove
694 residual diet. The samples were mounted on aluminum stubs, desiccated under vacuum, and sputter-
695 coated with gold before imaging with a TM4000 II Plus SEM (Hitachi, Tokyo, Japan). Salivary
696 sheath length (from apex to base) was measured, with 20 sheaths analyzed per treatment to ensure
697 statistical reliability.
698
699 **Statistical analysis**
700 The log-rank test (SPSS Statistics 19, Chicago, IL, USA) was used to determine the statistical
701 significance of survival distributions. Two-tailed unpaired Student's *t*-test (comparisons between
702 two groups) or one-way ANOVA test followed by Tukey's multiple comparisons test (comparisons
703 among three groups) was used to analyze the results of qRT-PCR, fecundity analysis, and host choice
704 analysis. The EPG data were first checked for the normality and homogeneity of variance, and those
705 not fitting a normal distribution were $\log_{10}$ transformed before Student's *t* test, as described in
706 previous studies [30]. Statistical tests, including Student's *t*-test and one-way ANOVA, and data
707 visualization were conducted in GraphPad Prism 9.
708
709 **Data availability**
710 All data is included in the manuscript and/or supporting information. The transcriptomic data have
711 been submitted to the National Genomics Data Center under accession number PRJCA025907. The
712 original blot images have been displayed in Fig. S29-S32.
713
714 **References**
715 1. Howe GA & Jander G (2008). Plant immunity to insect herbivores. *Annu Rev Plant Biol* 59, 41-

716 66.
717 2. Wang H, *et al*. (2024), Release brake and set plant defense in motion. *New Plant Prot* 1: e11.
718 3. Nürnberger T, Brunner F, Kemmerling B, & Piater L (2004) Innate immunity in plants and
719 animals: striking similarities and obvious differences. *Immunol Rev* 198(1):249-266.
720 4. Macho AP & Zipfel C (2014) Plant PRRs and the activation of innate immune signaling. *Mol*
721 *Cell* 54(2):263-272.
722 5. Zipfel C (2014) Plant pattern-recognition receptors. *Trends Immunol* 35(7):345-351.
723 6. Gust AA & Felix G (2014) Receptor like proteins associate with SOBIR1-type of adaptors to
724 form bimolecular receptor kinases. *Curr Opin Plant Biol* 21:104-111.
725 7. Adam D. Steinbrennera, *et al.* (2020) A receptor-like protein mediates plant immune responses
726 to herbivore-associated molecular patterns. *Proc Natl Acad Sci USA* 117(49):31510-31518.
727 8. Chinchilla D, Bauer Z, Regenass M, Boller T, & Felix G (2005) The *Arabidopsis* receptor kinase
728 FLS2 binds flg22 and determines the specificity of flagellin perception. *Plant Cell* 18(2):465-
729 476.
730 9. Zipfel C, *et al.* (2006) Perception of the bacterial PAMP EF-Tu by the receptor EFR restricts
731 *Agrobacterium*-mediated transformation. *Cell* 125(4):749-760.
732 10. Ron M & Avni A (2004) The receptor for the fungal elicitor ethylene-inducing xylanase is a
733 member of a resistance-like gene family in tomato. *Plant Cell* 16(6):1604-1615.
734 11. Tian T, *et al.* (2021) A salivary calcium-binding protein from *Laodelphax striatellus* acts as an
735 effector that suppresses defense in rice. *Pest Manag Sci* 77(5): 2272-2281.
736 12. Huang HJ, *et al.* (2019) Salivary DNase II from *Laodelphax striatellus* acts as an effector that
737 suppresses plant defence. *New Phytol* 224(2):860-874.
738 13. Chen CY, *et al.* (2019) An effector from cotton bollworm oral secretion impairs host plant
739 defense signaling. *Proc Natl Acad Sci USA* 116(28):14331-14338.
740 14. Xu HX, *et al.* (2019) A salivary effector enables whitefly to feed on host plants by eliciting
741 salicylic acid-signaling pathway. *Proc Natl Acad Sci USA* 116(2):490-495.
742 15. Chen CY & Mao YB (2020) Research advances in plant-insect molecular interaction. *F1000Res*
743 9(F1000 Faculty Rev):198.
744 16. Guiguet A, *et al.* (2016) Shared weapons of blood- and plant-feeding insects: Surprising
745 commonalities for manipulating hosts. *J Insect Physiol* 84:4-21.

746 17. Wu J & Baldwin IT (2009) Herbivory-induced signalling in plants: perception and action. *Plant*
747 *Cell Environ* 32(9):1161-1174.
748 18. Jiang YJ, Zhang CX, Chen RZ, & He SY (2019) Challenging battles of plants with phloem-
749 feeding insects and prokaryotic pathogens. *Proc Natl Acad Sci USA* 116(47):23390-23397.
750 19. Gao H，*et al*. (2023) The salivary chaperone protein NlDNAJB9 of *Nilaparvata lugens* activated
751 plant immune responses. *J Exp Bot* 74(21):6874-6888.
752 20. Guo H, *et al*. (2020) An aphid-secreted salivary protease activates plant defense in phloem. *Curr*
753 *Biol* 30(24): 4826-4836.
754 21. Bos JI, *et al*. (2010) A functional genomics approach identifies candidate effectors from the
755 aphid species *Myzus persicae* (green peach aphid). *PLoS Genet* 6(11):e1001216.
756 22. Zhang Y & Zeng L (2020) Crosstalk between ubiquitination and other post-translational protein
757 modifications in plant immunity. *Plant Commun* 1(4):100041.
758 23. Huang J*, et al.* (2020) *Phytophthora* effectors modulate genome-wide alternative splicing of
759 host mRNAs to reprogram plant immunity. *Mol Plant* 13(10):1470-1484.
760 24. Shan L*, et al.* (2008) Bacterial effectors target the common signaling partner BAK1 to disrupt
761 multiple MAMP receptor-signaling complexes and impede plant immunity. *Cell Host Microbe*
762 4(1):17-27.
763 25. Huang HJ*, et al.* (2016) Screening and functional analyses of *Nilaparvata lugens* salivary
764 proteome. *J Proteome Res* 15(6):1883-1896.
765 26. Huang HJ, *et al.* (2021) Identification of salivary proteins in the whitefly *Bemisia tabaci* by
766 transcriptomic and LC-MS/MS analyses. *Insect Sci* 28(5):1369-1381.
767 27. Gao H, *et al*. (2022) *Nilaparvata lugens* salivary protein NlG14 triggered defense response in
768 plants. *J Exp Bot* 73(22):7477-7487.
769 28. Mukhtar M, *et al*. (2011) Independently evolved virulence effectors converge onto hubs in a
770 plant immune system network. *Science* 333(6042):596-601.
771 29. Huang HJ*, et al.* (2023) Planthopper salivary sheath protein LsSP1 contributes to manipulation
772 of rice plant defenses. *Nat Commun* 14(1):737.
773 30. Lu S, *et al*. (2021) EPG-recorded feeding behaviors reveal adaptability and competitiveness in
774 two species of *Bemisia tabaci* (Hemiptera: Aleyrodidae). *J Insect Behav* 34: 26-40.
775 31. Yan ZW, *et al.* (2023) Endocytosis-mediated entry of a caterpillar effector into plants is

countered by Jasmonate. *Nat Commun* 14(1):6551.

32. Jones DA, *et al*. (1994) Isolation of the tomato Cf-9 gene for resistance to *Cladosporium fulvum* by transposon tagging. *Science* 266 (5186): 789-793 (1994).

33. Varshavsky A, *et al*. (2017) The ubiquitin system, autophagy, and regulated protein degradation. *Annu Rev Biochem* 86: 123-128.

34. Li L*, et al.* (2022) Independently evolved viral effectors convergently suppress DELLA protein SLR1-mediated broad-spectrum antiviral immunity in rice. *Nature Commun* 13(1):6920.

35. Takatsuka C*, et al.* (2004) 3-Methyladenine inhibits autophagy in tobacco culture cells under sucrose starvation conditions. *Plant Cell Physiol* 45: 265-274.

36. Tariqjaveed M*, et al.* (2021) Versatile effectors of phytopathogenic fungi target host immunity. *J Integr Plant Biol* 63(11):1856-1873.

37. Doblas VG, *et al.* (2018) Cell wall integrity signaling in plants: Malectin-domain kinases and lessons from other kingdoms. *Cell Surf* 3:1-11.

38. Albert I, *et al.* (2015). An RLP23–SOBIR1–BAK1 complex mediates NLP-triggered immunity. *Nat Plants* 1: 15140.

39. Li B, Lu D, & Shan L (2014) Ubiquitination of pattern recognition receptors in plant innate immunity. *Mol Plant Pathol* 15(7):737-746.

40. Chen Y, Song Y, Liu J, Xu G, & Dou D (2022) Ubiquitination of receptorsomes, frontline of plant immunity. *Int J Mol Sci* 23(6):2937.

41. Langin G, González-Fuente M, & Üstün S (2023) The plant ubiquitin–proteasome system as a target for microbial manipulation. *Annu Rev Phytopathol* 61:351-375.

42. Rosas-Diaz T*, et al.* (2018) A virus-targeted plant receptor-like kinase promotes cell-to-cell spread of RNAi. *Proc Natl Acad Sci USA* 115(6):1388-1393.

43. Irieda H*, et al.* (2019) Conserved fungal effector suppresses PAMP-triggered immunity by targeting plant immune kinases. *Proc Natl Acad Sci USA* 116(2):496-505.

44. Qin J*, et al.* (2018) The Xanthomonas effector XopK harbours E3 ubiquitin-ligase activity that is required for virulence. *New Phytol* 220(1):219-231.

45. Xu FQ, Xue HW (2019) The ubiquitin-proteasome system in plant responses to environments. *Plant Cell Environ* 42(10):2931-2944.

46. Katoh K & Standley DM (2013) MAFFT multiple sequence alignment software version 7:

806 improvements in performance and usability. *Mol Biol Evol* 30(4):772-780.
807 47. Kozlov AM, Darriba D, Flouri T, Morel B, & Stamatakis A (2019) RAxML-NG: a fast, scalable
808 and user-friendly tool for maximum likelihood phylogenetic inference. *Bioinformatics*
809 35(21):4453-4455.
810 48. Livak, K.J., and Schmittgen, T.D. (2001). Analysis of relative gene expression data using real-
811 time quantitative PCR and the $2^{-\Delta\Delta CT}$ method. *Methods* 25, 402-408.
812 49. Xu HJ*, et al.* (2015) Two insulin receptors determine alternative wing morphs in planthoppers.
813 *Nature* 519(7544):464-467.
814 50. Kim, D., Langmead, B., and Salzberg, S.L. (2015). HISAT: A fast spliced aligner with low
815 memory requirements. *Nature Methods* 519(7544):464-467.
816 51. Li, H. (2009). The Sequence Alignment/Map format and SAMtools. *BIOINFORMATICS -*
817 *OXFORD*.
818 52. Trapnell, C., Roberts, A., Goff, L., Pertea, G., Kim, D., Kelley, D.R., Pimentel, H., Salzberg,
819 S.L., Rinn, J.L., and Pachter, L. (2012). Differential gene and transcript expression analysis of
820 RNA-seq experiments with TopHat and Cufflinks. *Nature Protocols* 7, 562-578.
821 53. Wang, L., Feng, Z., Wang, X., Wang, X., and Zhang, X. (2010). DEGseq: an R package for
822 identifying differentially expressed genes from RNA-seq data. *Bioinformatics* 26, 136-138.
823 54. Chen, C., Chen, H., Zhang, Y., Thomas, H.R., Frank, M.H., He, Y., and Xia, R. (2020). TBtools:
824 an integrative toolkit developed for interactive analyses of big biological data. *Mol Plant* 13,
825 1194-1202.
826 55. Wang, N., Yin, Z., Zhao, Y., Wang, J., Pei, Y., Ji, P., Daly, P., Li, Z., Dou, D., and Wei, L. (2022).
827 An F-box protein attenuates fungal xylanase-triggered immunity by destabilizing LRR-RLP
828 NbEIX2 in a SOBIR1-dependent manner. *New Phytol* 236(6):2202-2215.
829

830 **Acknowledgements**

831 This project has received funding from the National Natural Science Foundation of China
832 (32422075: H.J.H.; U23A6006: J.P.C and C.X.Z.), National Key Research and Development
833 Program of China (2021YFD1401100: H.J.H, C.X.Z.), and the Natural Science Foundation of
834 Zhejiang Province (LDQ24C140001: H.J.H).
835

Author Contributions Statement

H-JH, J-ML, C-XZ, and J-PC planned and designed the research. XW, J-BL, Y-ZW, and H-JH performed experiments and analyzed data. X-HZ provided the EV plants. H-JH and XW drafted the manuscript.

Competing Interests Statement

The authors declare no competing interests.

845 **Figure Legends**

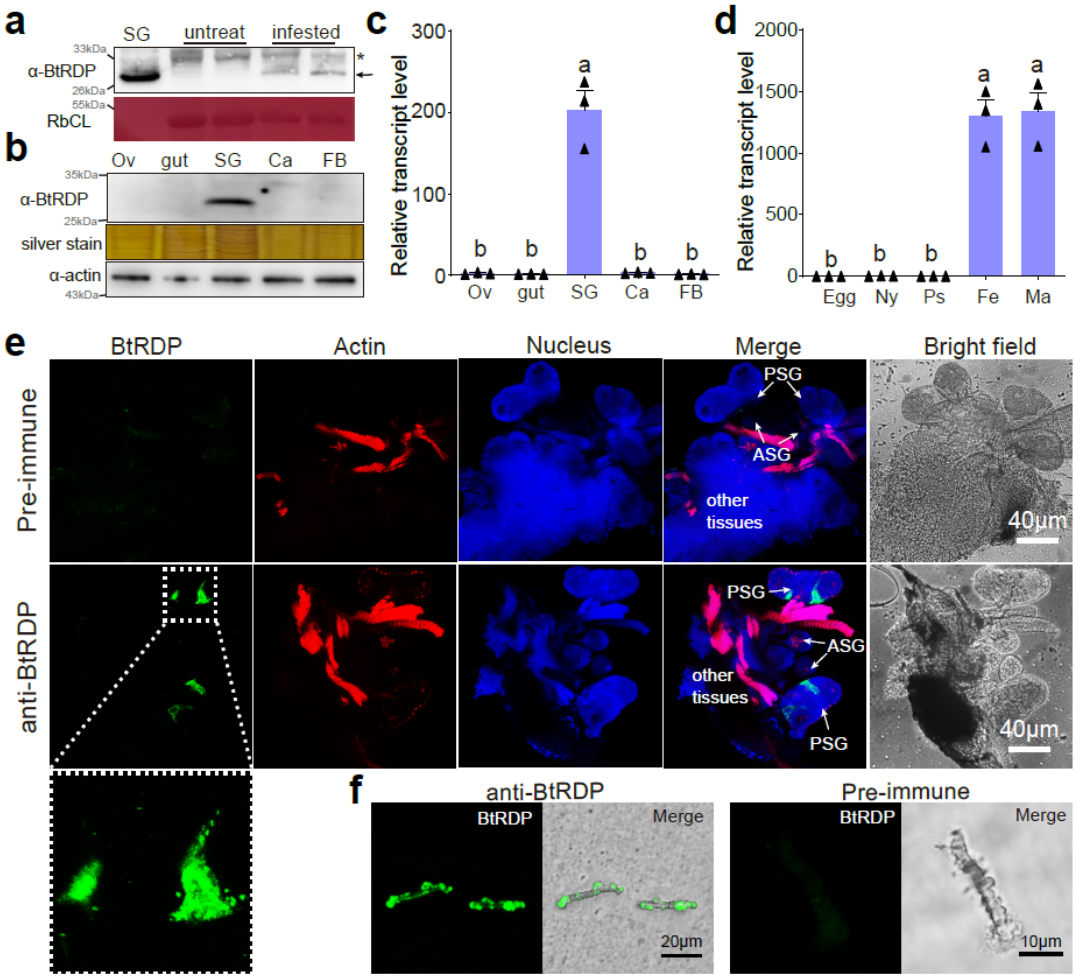

846

847 **Fig. 1. BtRDP is a salivary protein and secreted into plants.** (**a**) Detection of BtRDP in *Nicotiana*
848 *tabacum* plants. The untreated and *Bemisia tabaci*-infested tobacco plants, as well as the salivary
849 gland samples, are collected for western-blotting assays. Asterisk indicates non-specific binding.
850 Rubisco staining (RbcL) is conducted to visualize the amount of sample loading. **(b**, **c)** Detection
851 of BtRDP in different tissues by western-blotting and qRT-PCR assays. Ov, ovary; SG, salivary
852 gland; Ca, carcass; FB, fat body. Silver staining and anti-actin serum are used to visualize the sample
853 loading. (**d**) Expression patterns of BtRDP in different development stages. Ny, nymph; Ps,
854 pseudopupa; Fe, female; Ma, male. *B. tabaci tubulin* is used as an internal control. The relative
855 quantitative method ($2^{-\Delta\Delta Ct}$) is used to evaluate the quantitative variation. Data are presented as mean
856 values ± SEM (n= 3 independent biological replicates). Different lowercase letters indicate
857 statistically significant differences at the $P < 0.05$ level according to one-way ANOVA test followed
858 by Tukey's multiple comparisons test. **(e, f)** Immunohistochemical staining of BtRDP in salivary
859 glands **(e)** and salivary sheath secreted from *B. tabaci* **(f)**. The salivary gland and its nearby tissues

are dissected and incubate with anti-BtRDP serum or pre-immune serum conjugated with Alexa Fluor™ 488 NHS Ester (green) and actin dye phalloidinrhodamine (red). The nucleus is stained with DAPI (blue). PSG, principal salivary gland; ASG, accessory salivary gland. The lower images represent the enlarged images of the boxed area in the upper image. Experiments are repeated thrice for **(a** and **b)**, while twice for **(e** and **f)**. Similar results are observed and representative images are displayed.

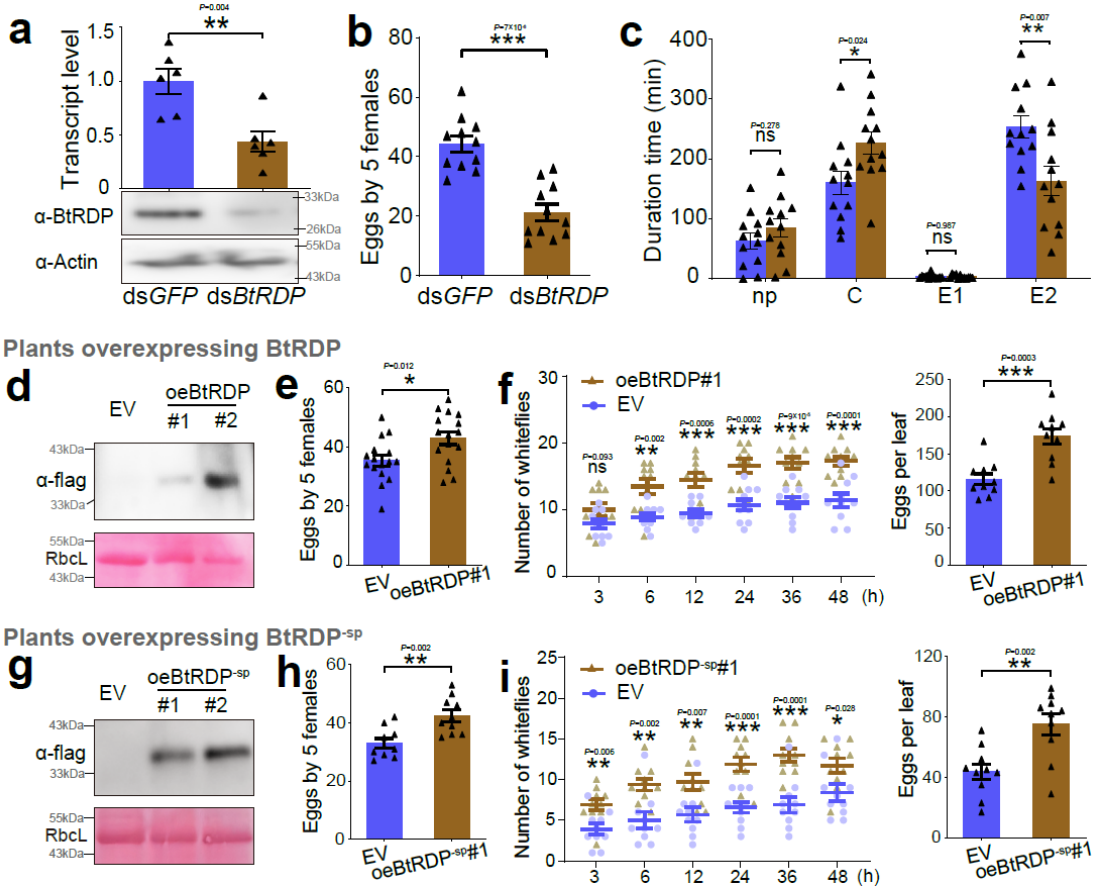

Fig. 2. Effects of BtRDP on *Bemisia tabaci*. (**a**) Treating *B. tabaci* with ds*BtRDP* significantly reduces the transcript and protein level of target gene. The ds*GFP*-treated *B. tabaci* is used as a control. **(b–c)** Effects of *BtRDP* knockdown on insect reproduction **(b)** and feeding behavior **(c)**. Electrical penetration graph (EPG) is used to monitor the insect feeding behavior, which can be classified into nonpenetration (np), pathway duration (C), phloem salivation (E1) and phloem ingestion (E2) phases. All EPG recordings are performed for 8 h. Typical EPG waveforms are displayed in Fig. S7. **(d-f)** Insect performance on transgenic plants overexpressing BtRDP (oeBtRDP). **(d)** Detection of BtRDP in transgenic *Nicotiana tabacum* overexpressing a complete

876 coding region of *BtRDP*. The empty vector (EV) plants are used as the control. The flag tag is fused
877 to the C-terminal ends of recombinant proteins. **(e)** Comparison of insect reproduction on
878 oeBtRDP#1 and EV plants. Five *B. tabaci* individuals are confined to indicated plants for 3 days,
879 and the oviposited eggs are counted. **(f)** Attraction of oeBtRDP#1 and EV leaves to *B. tabaci* in a
880 two-choice equipment. A group of 40 female *B. tabaci* are released into a device containing
881 oeBtRDP#1 and EV leaves. The number of insects settling on each leaf is counted. After 48 h, the
882 number of eggs on each leaf is counted. **(g-i)** Insect performance on transgenic plants overexpressing
883 $BtRDP^{-sp}$ ($oeBtRDP^{-sp}$). **(g)** Detection of $BtRDP^{-sp}$ in transgenic *N. tabacum* overexpressing BtRDP
884 without a signal peptide. The insect reproduction **(h)** and settlement **(i)** on $oeBtRDP^{-sp}$ transgenic
885 plants are recorded. The EPG data are first checked for normality and homogeneity of variance, and
886 data not fitting a normal distribution are subjected to log10 transformation. Data are presented as
887 mean ± SEM. Statistical significance in panels **(a)**, **(b)**, **(c)**, **(e)**, **(f)**, **(h)**, and **(i)** was assessed using
888 two-tailed unpaired Student's *t*-tests. ***$P < 0.001$; **$P < 0.01$; *$P < 0.05$; ns, not significant.
889 Western-blotting assays are repeated thrice with the similar results.

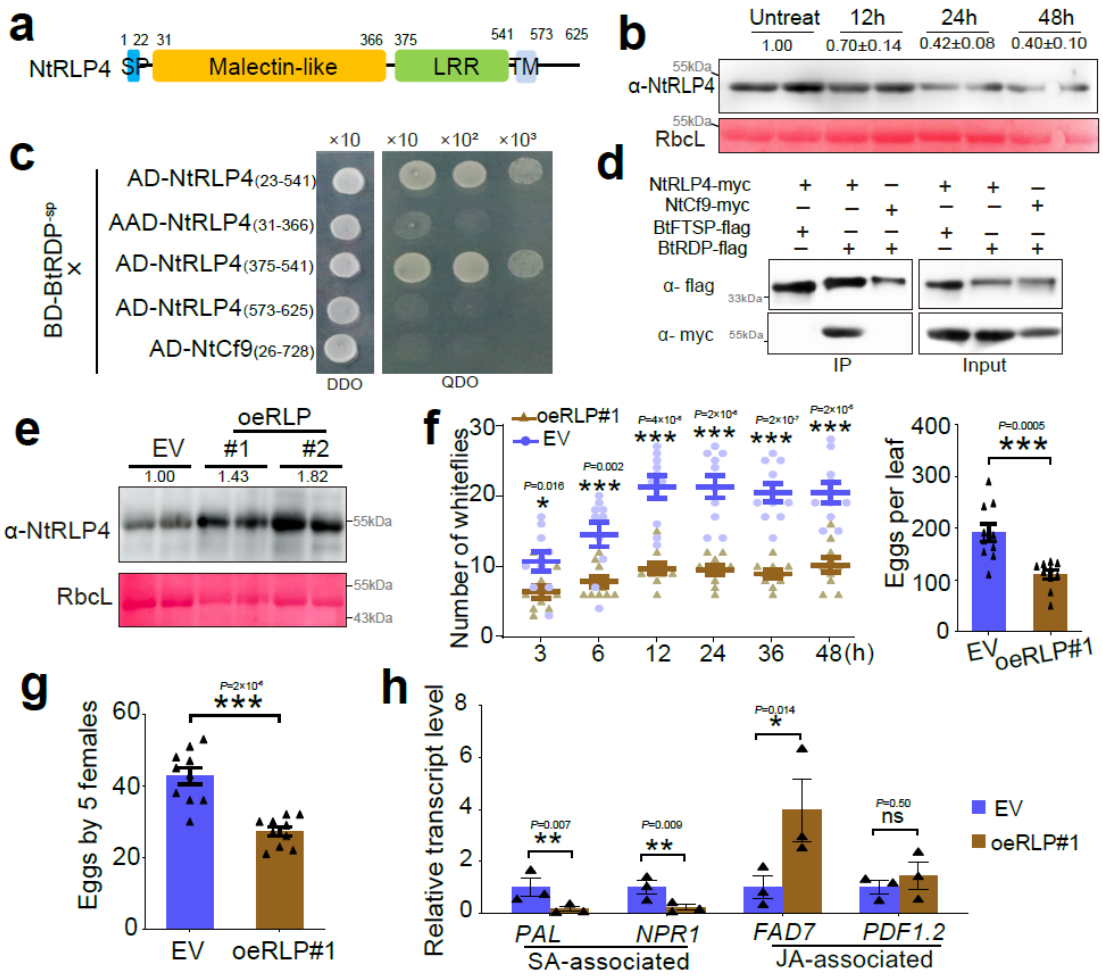

Fig. 3. NtRLP4 interacts with BtRDP and confers plant resistance to *Bemisia tabaci*. (a) Domain organization of NtRLP4. NtRLP4 contains a predicted N-terminal signal peptide (SP), a malectin-like domain, a LRR domain, and a transmembrane domain (TM). **(b)** The protein level of NtRLP4 in response to *B. tabaci* infestation. The untreated *Nicotiana tabacum* is used as a negative control. Four independent biological replicates are performed, and the representative images are displayed. The band density is measured using ImageJ. The density values from 4 biological replicates are calculated and the mean value in the controls is set at 1.0. **(c)** Yeast two hybrid assays showing the interaction between BtRDP and NtRLP4. The different combinations of constructs are transformed into yeast cells, and are grown on the selective medium SD/-Trp/-Leu (DDO), and the interactions are tested with SD/-Trp/-Leu/-His/-Ade (QDO). **(d)** Co-immunoprecipitation assay showing the interaction between BtRDP and NtRLP4. Total proteins are extracted from *N. benthamiana* leaves transiently co-expressing NtRLP4-myc/NtCf9-myc with BtFTSP-flag/BtRDP-flag. All genes are expressed with a complete coding region, and the myc/flag tags are fused at the C-terminus. Precipitation is performed using flag beads. The samples are probed with anti-flag and

905 anti-myc antibodies for immunoblotting analysis. **(e–h)** Analysis of transgenic *N. tabacum*
906 overexpressing NtRLP4 (oeRLP). **(e)** Detection of NtRLP4 level in oeRLP plants. The empty vector
907 (EV) plant is used as a control. Two independent oeRLP lines are selected. The samples are probed
908 with an anti-NtRLP4 antibody. Rubisco staining (RbcL) is used to visualize the amount of sample
909 loading. **(f)** Attraction of oeRLP#1 and EV leaves to *B. tabaci* in a two-choice equipment. A group
910 of 40 female *B. tabaci* are released into a device containing oeRLP#1 and EV leaves. The number
911 of insects settling on each leaf is counted at each time point. After 48 h, the number of eggs on each
912 leaf is counted. **(g)** Comparison of insect reproduction on oeRLP#1 and EV plants. Five *B. tabaci*
913 individuals are confined to indicated plants for 3 days, and the oviposited eggs are counted. **(h)**
914 Relative transcript levels of salicylic acid (SA)- and jasmonic acid (JA)-associated genes in
915 oeRLP#1 and EV plants. PAL, phenylalanine ammonia lyase; NPR1, nonexpressor of pathogenesis-
916 related protein 1; FAD7, fatty acid desaturase 7; PDF1.2, plant defensin 1.2. Two independent
917 biological replicates are performed in **(d)** and **(e)**. Data in **(f)**, **(g)**, and **(h)** are presented as mean
918 values ± SEM. For insect bioassays in (**f**) and (**g**), n= 10 independent biological replicates. For qRT-
919 PCR in (**h**), n= 3 independent biological replicates. *P*-values are determined by two-tailed unpaired
920 Student's *t* test. ***$P < 0.001$; **$P < 0.01$; *$P < 0.05$; ns, not significant.

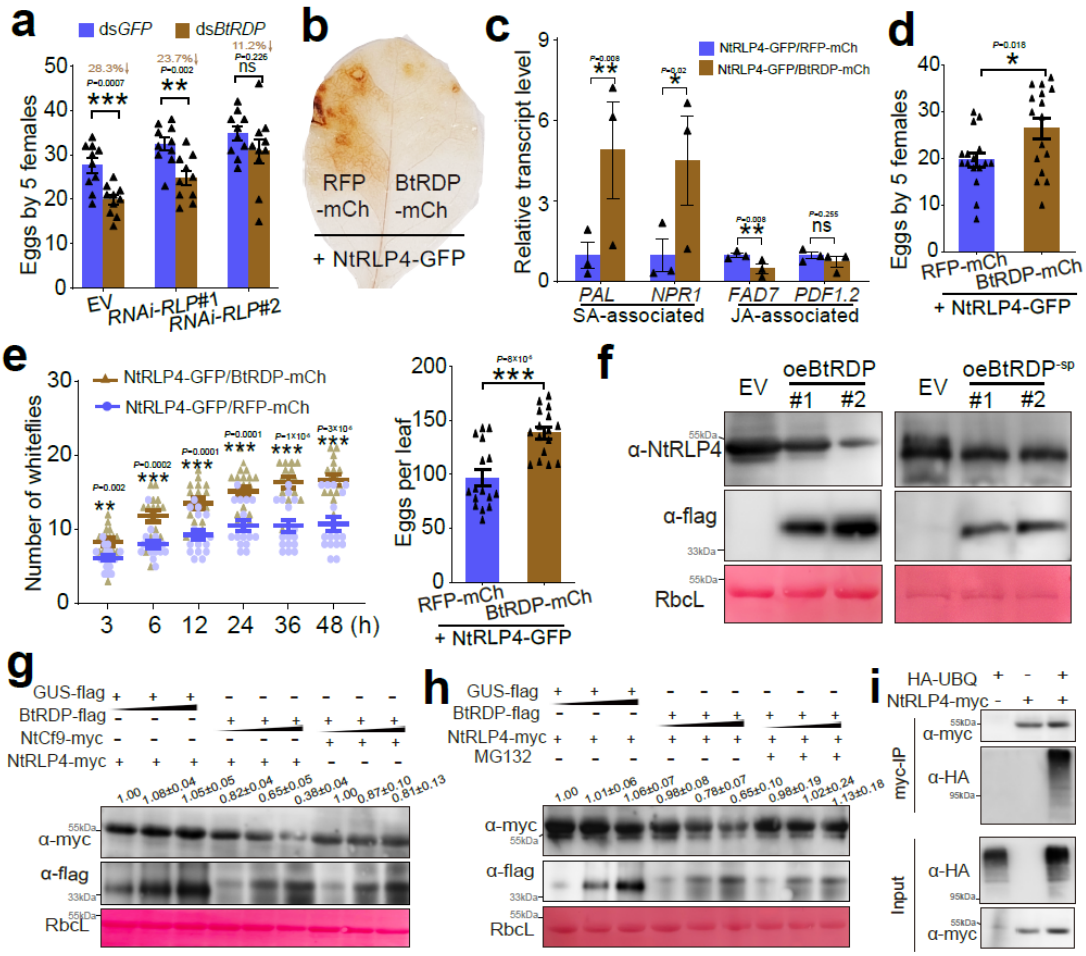

Fig. 4. BtRDP suppress plant defenses by promoting NtRLP4 degradation. (a) Effects of ds*BtRDP* suppression on insect reproduction (n= 10 independent biological replicates) when feeding on empty vector (EV) and NtRLP4-silenced (*RNAi-RLP*) transgenic *Nicotiana tabacum*. **(b)** Transient overexpressing BtRDP-mCherry attenuates H_2O_2 accumulation caused by NtRLP4-GFP overexpression. *N. tabacum* co-expressing RFP-mCherry and NtRLP4-GFP is used as a control. All genes are expressed with a complete coding region. The experiment is repeated 5 times with the similar results. **(c)** Relative transcript level of salicylic acid (SA)- and jasmonic acid (JA)-associated genes in BtRDP-mCherry/NtRLP4-GFP and RFP-mCherry/NtRLP4-GFP plants (n=3 independent biological replicates). PAL, phenylalanine ammonia lyase; NPR1, nonexpressor of pathogenesis-related protein 1; FAD7, fatty acid desaturase 7; PDF1.2, plant defensin 1.2. **(d)** Comparison of insect reproduction (n= 16 independent biological replicates) on transient-expressed BtRDP-mCherry/NtRLP4-GFP and RFP-mCherry/NtRLP4-GFP plants. **(e)** Attraction of BtRDP-mCherry/NtRLP4-GFP and RFP-mCherry/NtRLP4-GFP leaves to *B. tabaci* in a two-choice equipment (n= 16 independent biological replicates). The number of eggs on each leaf is counted at

936 48 h post insect release. (**f**) Effects of BtRDP and BtRDP^{-sp} overexpression on NtRLP4
937 accumulation. Transgenic oeBtRDP (left) and oeBtRDP^{-sp} (right) plants are probed with anti-
938 NtRLP4 and anti-flag antibodies for immunoblotting analysis. The experiments are repeated twice
939 with the similar results. **(g)** Degradation of NtRLP4 by BtRDP in *N. benthamiana* leaves. NtRLP4-
940 myc and BtRDP-flag are transiently co-expressed in *N. benthamiana* plants through *Agrobacterium*
941 infiltration. *Agrobacterium* carrying NtCf9-myc and GUS-flag are used as negative controls. **(h)**
942 Effects of 26S proteasome inhibitor (MG132) on NtRLP4 accumulation. Co-infiltrated leaves are
943 treated with MG132 at 24 h post injection. The samples are probed with anti-flag and anti-myc
944 antibodies for immunoblot analysis. Rubisco staining (RbcL) is conducted to visualize the amount
945 of sample loading. The small triangle indicates the different concentrations of *Agrobacterium*
946 (OD_{600} = 0.05, 0.3, and 1.0). **(i)** NtRLP4 is ubiquitinated *in planta*. NtRLP4-myc is co-expressed
947 transiently with HA-UBQ in *N. benthamiana* leaves. Extracted total proteins are
948 immunoprecipitated by anti-myc beads and immunoblotted with anti-myc or anti-HA antibody.
949 Experiments are repeated thrice for (**g**) and (**h**), while twice for (**i**). Band density is measured using
950 ImageJ. The density values from three biological replicates are calculated and the mean value in the
951 first lane is set at 1.0. Data are presented as mean values ± SEM. *P*-values are determined by two-
952 tailed unpaired Student's *t* test. ***$P < 0.001$; **$P < 0.01$; *$P < 0.05$; ns, not significant.

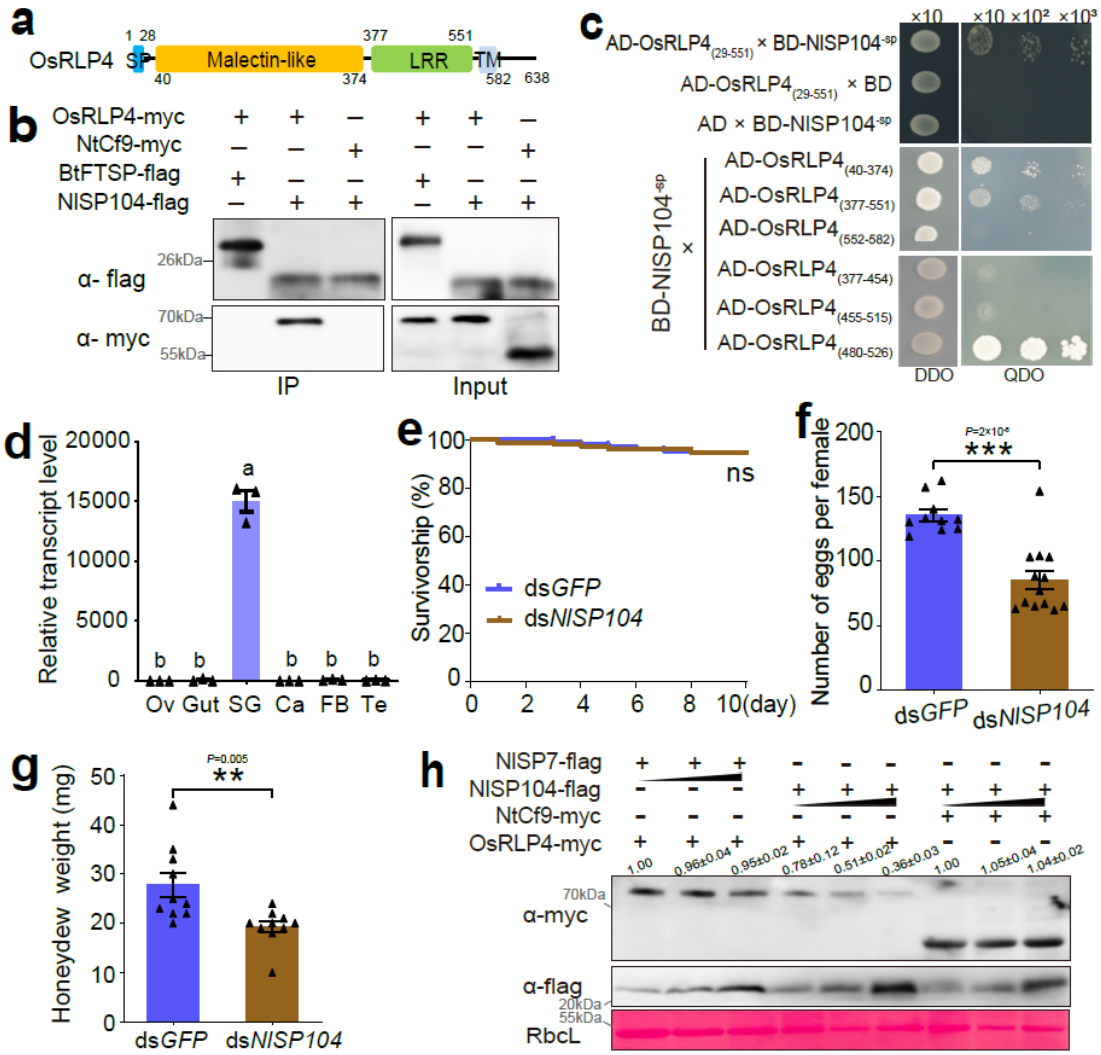

Fig. 5. Rice RLP4 are targeted by salivary protein NlSP104 from *Nilaparvata lugens*. (a) Domain organization of *Oryza sativa* RLP4 (OsRLP4). **(b, c)** Yeast two-hybrid and Co-IP assays showing the interaction between OsRLP4 and NlSP104. All genes are expressed with a complete coding region in Co-IP assays, while NlSP104 without a signal peptide is used in yeast two-hybrid assays. Experiments in (**b**) are repeated twice with the similar result. **(d)** The expression patterns of *NlSP104* in different *N. lugens* tissues. Te, testis; Ov, ovary; SG, salivary gland; Ca, carcass; FB, fat body. Data are presented as mean values ± SEM (n= 3 independent biological replicates). Different lowercase letters indicate statistically significant differences at $P < 0.05$ level according to one-way ANOVA test followed by Tukey's multiple comparisons test. **(e-g)** Effects of dsRNA treatment on insect survivorship (**e**), reproduction (**f**), and honeydew excretion (**g**). For survivorship analysis, a group of 30 *N. lugens* are reared in a cage. Three independent biological replications are performed. Differences in survivorship between the two treatments are tested by log-rank test. ns, not significant.

966 For reproduction analysis, n= 10 and 13 individuals are tested in ds*GFP*- and ds*NlSP104*-treatment,
967 respectively. The sterile females are excluded from data analysis. For honeydew analysis, n= 10
968 independent biological replicates. *P*-values in **(f)** and **(g)** are determined by two-tailed unpaired
969 Student's *t* test. ***$P < 0.001$; **$P < 0.01$. **(h)** Effect of NlSP104 on the accumulation of transient-
970 expressed OsRLP4. OsRLP4-myc is agro-injected into *Nicotiana benthamiana* together with
971 different concentrations of NlSP104-flag and NlSP7-flag. NtCf9-myc is used as a negative control.
972 The small triangle indicates the different concentrations (OD_{600} = 0.05, 0.3, and 1.0) of
973 *Agrobacterium*. Rubisco staining (RbcL) is conducted to visualize the amount of sample loading.
974 Experiments are repeated three times with the similar results. Band density is measured using
975 ImageJ. The density values from three biological replicates are calculated with the mean value in
976 the first lane being set at 1.0.

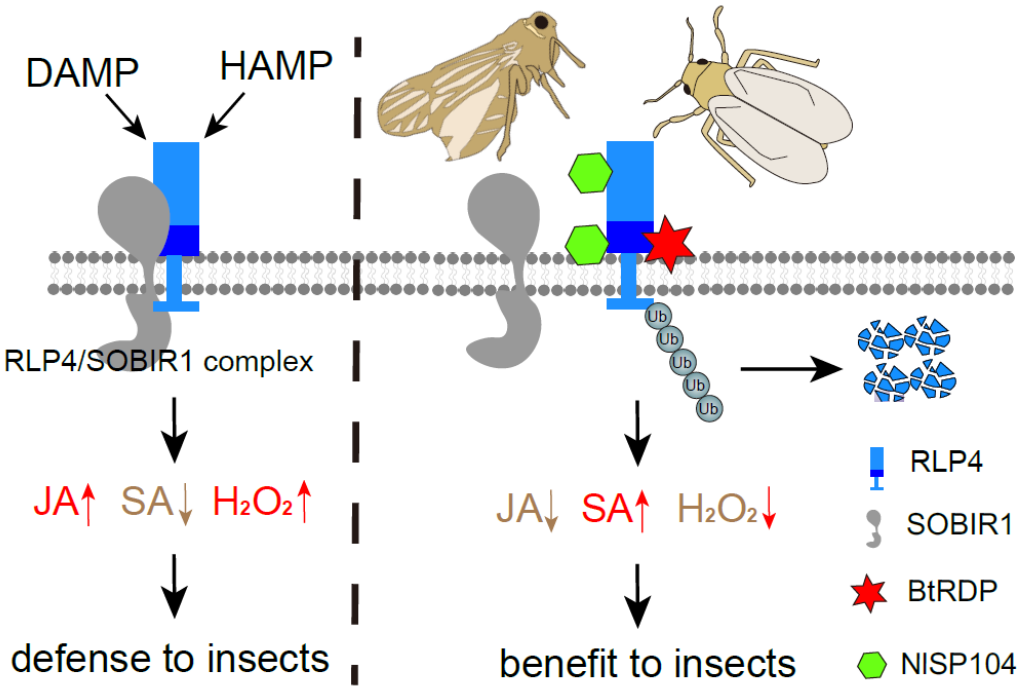

977

978 **Fig. 6. The proposed model for the suppression of receptor-like proteins (RLPs)-mediated**
979 **plant defenses by salivary effectors.** Host plants employ pattern-recognition receptors (PRRs) to
980 detect various damage-associated molecular patterns (DAMPs) and herbivore-associated molecular
981 patterns (HAMPs) triggered by insect feeding. The RLP4/SOBIR1 complex plays a vital role in
982 initiating pattern-triggered immunity (PTI), including H_2O_2 burst, upregulation of jasmonic acid
983 (JA), and downregulation of salicylic acid (SA), which hinders insect feeding. The whitefly *Bemisia*
984 *tabaci* and planthopper *Nilaparvata lugens* independently evolved salivary proteins that targeted

985 plant RLP4. *B. tabaci* salivary sheath protein BtRDP interacts with the leucine-rich repeat (LRR)
986 domain of RLP4 from *Nicotiana tabaci* and *Solanum lycopersicum*, while *N. lugens* NlSP104 targets
987 both the LRR domain and the malectin-like domain of *Oryza sativa* RLP4. These interactions
988 promote the ubiquitin-dependent degradation of RLP4, thereby disrupting the stability of the
989 RLP4/SOBIR1 complex. The presence of salivary effectors causes a hormonal shift and suppresses
990 the H_2O_2 burst, finally favoring insect feeding.
991
992